Rock Mechanics

The 19th International Mining Congress and Fair of Turkey, IMCET2005, İzmir, Turkey, June 09-12, 2005

The Influence of Resin Thickness on Bolt Bending

N. Aziz, J. Hossein, M.S.N. Hadi
School of Civil, Mining and Environmental Engineering, University of Wollongong, NSW, Australia, 2522

ABSTRACT: Load transfer mechanism of bolt has been the subject of increased research for more than three decades, particularly with regard to resin thickness. The influence of increased resin thickness on axially loaded bolts has been widely reported and documented, however there remains a lack of clear understanding of the bolt-resin and rock interaction with different resin thickness particularly when the bolt is sheared. Accordingly, this study is aimed to examine the effect of resin thickness on the bolt-grout-concrete interaction under double shearing conditions. The bending and shearing characteristics of bolts were conducted both in the laboratory and in 3D numerical simulation, and with and without different pretension loads. Both the strength of the concrete and bolt pretension load had been found to have major influence on the shear resistance and shear displacement of the reinforced concrete in all resin thickness. Also, the strength of the surrounding concrete was found to play a greater role than the grout thickness, particularly when the bolt is in pretension.

1 INTRODUCTION

Fully grouted rock bolts are widely used in both civil and geotechnical engineering constructions as reinforcement elements. A fully grouted bolt in intersection with a joint plane increases the resistance to shear across the joint. Many researchers have undertaken significant research in the numerical and laboratory methods to study the mechanical behaviour of bolted rock joints, and much of the theoretical studies were undertaken using various available approaches such as the finite element and finite difference methods. Bolts can be installed as passive or as active pre-tensioned support element. However, there is an ongoing debate on the methodology of bolt installation with regard to bolt pretensioning. When bolts installed in underground excavations or in surface mining, they are loaded both axially and laterally depending on the movement direction of the reinforced unstable rock block.

Research on sheared surface reinforcement has been the subject of research that is being pursued with increasing vigor in recent years, ever since the benefits of full encapsulation was realized. Numerous experimental and numerical studies were undertaken over the past three decades to investigate the mechanical behaviour of fully grouted rock bolt in rocks and in bolt shearing conditions. The works of Dulacska (1972), Bjurstrom (1974) Azuar (1977), Hass (1976,1981), Hibino and Motojima (1981), Dight (1982), Spang and Egeer (1990), Ferrero (1995), Pellet and Boulon (1998), Kharchafi and et al (1998), and Grasselli (2004), Aziz et al (2004) are well documented.

The effect of resin thickness is one of most important factors to transfer the maximum load from bolt to the rock. When a bolt is loaded axially by pushing/pulling through the resin thickness, thicker resin layers show minimum load transfer. Several authors conducted this research in the past, (Fabjanczyk, Hurt, & Hindmars, (1992); Aziz and Webb (2003); Aziz 2004). However, to understand the effect of resin thickness while bolt is laterally loaded under shearing effect, there appears to be a lack of reporting on the subject. Thus, in this study the laboratory tests and numerical simulations were conducted to she light on this aspect of bolt -resin and rock interaction. Double shear laboratory tests were carried out only in 27 mm hole diameter and 22 mm bolt diameter. The laboratory study was then supported by extensive numerical simulations with different resin thickness, material strength and bolt pretensioning was undertaken. This paper highlights the effective role that the resin thickness in different

rock strengths and pretensions could play in rock reinforcement.

2 LABORATORY TESTS

The general set up of the double shear box unit in a testing machine is shown in Figure 1, Double-jointed concrete blocks were cast for each double shearing test. Two different strengths concrete blocks, at 20MPa and 40MPa, were cast to simulate two different strength rocks. The concrete/bolt assembly was then mounted in a steel frame shear box specifically fabricated for this purpose. A base platform that fitted into the bottom ram of the Instron Universal Testing Machine, capacity 500 kN, was used to hold the shear box. A predetermined tensile load was applied to the bolt prior to shear loading. This acted as a compressive/confining pressure to simulate different forces on the joints within the concrete. The three nominated tension forces used were 20kN, 50kN and 80kN. Axial tensioning of the bolt was accomplished by tightening simultaneously the nuts on both ends of the bolt. The applied axial loads were monitored by two hollow load cells mounted on the bolt on either side of the block. Figure 2 and 3 show the load deflection trend in 20 and 40 MPa concretes respectively in different pretensions installed in 27 mm hole diameter. As they show higher concrete strength and pretension load leads higher shear resistance. Figure 4 displays yield load increase as a function of pretension load in concrete 20 MPa. This relation behaves as a power function. The axial load on the bolt increased with increasing the shear load. The rate of axial load increase is on the rise once the elastic range is exceeded.

Figure 5 shows the relationship between the axial loads developed and shear displacement in high strength bolt (ultimate tensile strength around 330 kN) installed in 40 MPa concrete. From the graph it can be seen that the axially induced load on the bolt at low level of pretensioning, is higher than that of high level of pretensioning. The possible reason is attributed to lower confinement resistance, causing the bolt to deform much more readily, with an increase in axial load of the bolt as the bolt is clamped at both ends.

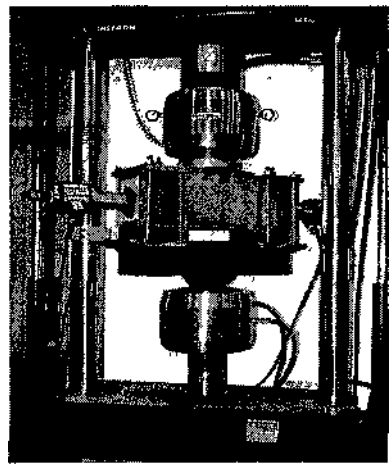

Figure 1.General set up of double shear box in Instron machine

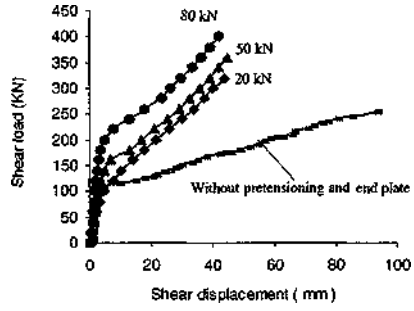

Figure 2. Shear load -shear displacement trend in bolt surrounded with 20 MPa concrete and 27 mm hole diameter

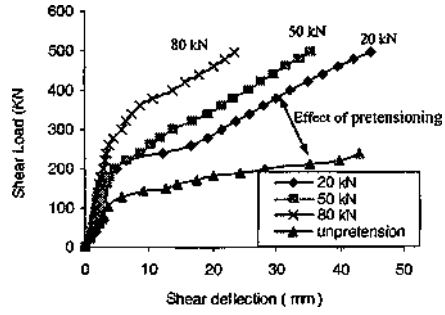

Figure 3. Shear load versus shear deflection in different pretensioning with 40 MPa concrete and 27 mm hole diameter

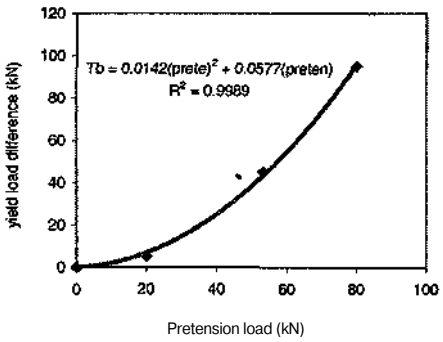

Figure 4. Yield load increase versus pretension load in 20 MPa concrete

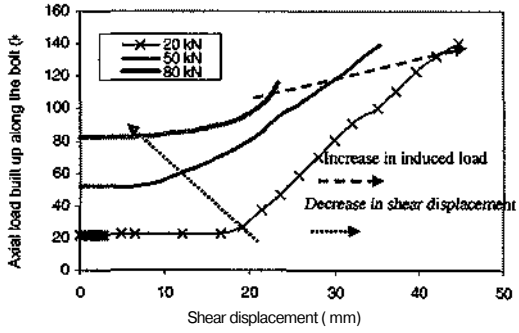

Figure 5. Axial load build up along the bolt as a function of shear displacement in 40 MPa concrete and different pretension loads

3 3D NUMERICAL SIMULATION

3D simulation of the bolt shearing process was conducted using ANSYS version 8.1 package. Numerical simulations were carried out in 20 and 40 MPa concrete and in different resin thickness. The objectives were to examine the strains and stresses developed in different resin thickness and various pretension loads of 20, 50, and 80 kN. A large number of numerical models were created, to describe different resin thickness in different pretensions and rock strength. The confirmation of the numerical simulations with laboratory results is shown in Figures 6. It can be seen that the numerical simulations were found to be in close agreement with the experimental results.

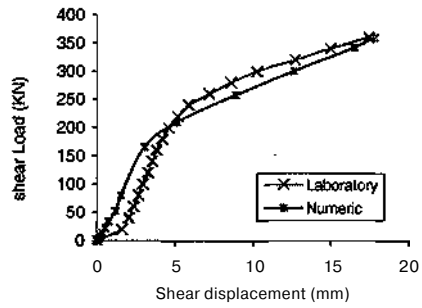

Figure 6. Load-deflection in 20 kN pretension load in 40 MPa concrete

Following the system calibration, a number of 3D numerical simulations were then carried out in 20 and 40 MPa concrete blocks in both un-pretension and pretension loads of 20, 50 and 80 kN. This FEM of the reinforced structure subjected to the shear loading was used to examine the behavior of bolted rock joints, such as; strength of material, pretensioning and resin thickness. Parameters considered were, the three governing materials (steel, grout, and rock) with two interfaces (bolt - grout and grout - rocks). Using (ANSYS, Version 8.1), it was possible to simulate specifically the elasto-plastic materials and contact interfaces behaviors. The stress-strain relationship of steel was assumed as bilinear kinematics hardening model and the modulus of elasticity of strain hardening was accounted as one hundredth of the original value. Figure 7 shows finite element mesh for a quarter of the model. The elastic properties of materials are displayed in table 1.

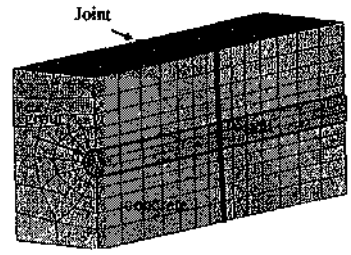

Figure 7. Three-dimensional meshed model of a quarter section of the composite concrete/resin and bolt

Table 1: Elastic material properties

Material	UCS (MPa)	E (GPa)	Poisson's Ratio
Concrete 1	20	20	0.2
Concrete 2	40	32	0.2
Resin Grout	60	12	0.25
Steel	330kN	200	0.3

Numerical modeling was carried out in different resin thickness of, 1.5, 2.5 and 5 mm, in borehole diameters of 25, 27 and 32 mm respectively. Figures 8 and 9 show the created gap among interfaces in thin and thick resin layer.

From the figures it can be seen that with increasing the shear load, the grout layer becomes separated from the bolt and concrete in the tension zones and is compressed at compression zone. The separation gap occurred in all resin thickness. The gap in thin resin layer is more extensive than the thick resin layer and also changes in stresses, strains and displacement along the bolt and surrounding materials are different. With the bolt is bent, and the gap is increased, and the contact pressure is removed. However, at the compression zones in the vicinity of shear joint, reaction stress will result. Because of extensive output results from numerical simulations, only a few figures are provided in this paper. Figure 10 shows the value of induced strain along the bolt in shear direction around the grout 1.5 mm thick. Compared to thick resin the level of strain, in both tension and compression zones, is higher and the resin is fragmented with low shear load.

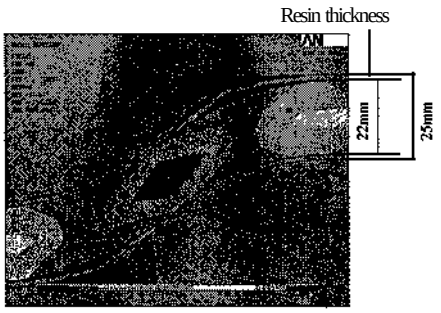

Figure 8- Shear stress and created gap in 1.5 mm resin thickness with 20 MPa concrete without pretensioning

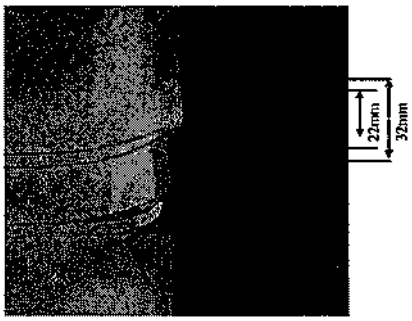

Figure 9. Model deformation and created gap between interfaces in 5 mm resin thickness

Figure 11 shows the plastic strain in shear direction along the thick resin layer in 20 MPa concrete. The value of the strain in the vicinity of the shear joint, is high, thus causing a complete damage in resin layer. Figure 12 displays the value of induced strain along the bolt axis through the resin in 40 MPa concrete with 80 kN pretension.

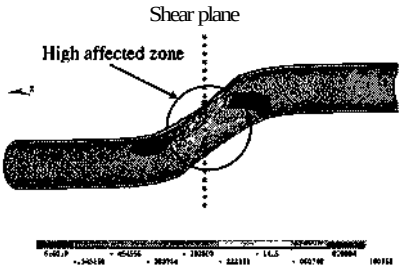

Figure 10. Plastic strain in shear direction along thin grout layer in 20 MPa without pretensioning

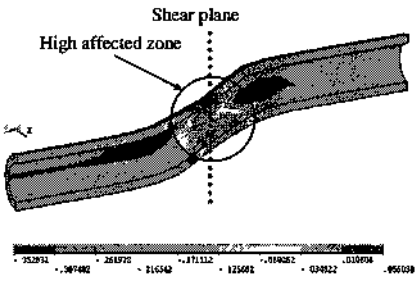

Figure 11. Plastic strain in shear direction along thick grout layer in 20 MPa concrete without pretensioning

Figure 13 shows, there is a dramatic increase in strain change in the resin layer in the vicinity of shear joint.

The value of strain, at both the axial and lateral directions in the vicinity of shear joint plane, was above the elastic yield point of the resin, which is a clear indication that the strength of resin is exceeded.

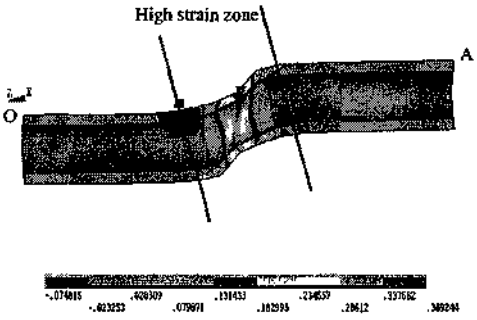

Figure 12. Axial plastic strain along the thick resin layer in 40 MPa concrete with 80 kN pretensioning

Figure 14 shows the trend of induced stress and concrete deflection along the bolt axis through the concrete block. It shows that the stresses around the concrete block are high at the edges in the vicinity of shear joint, thus inducing longitudinal fractures in the concrete blocks. This was also observed at the experimental results, and was common to all resin thickness and concrete strengths.

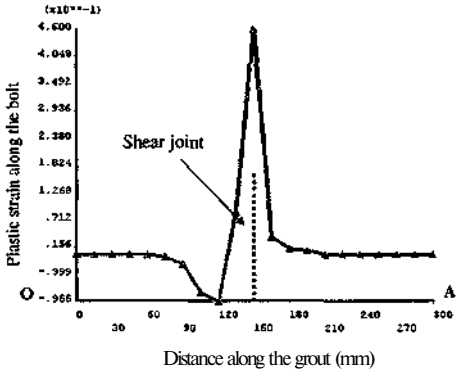

Figure 13. Plastic strain along the thick resin layer in axial direction of the bolt in 40 MPa concrete without pretensioning

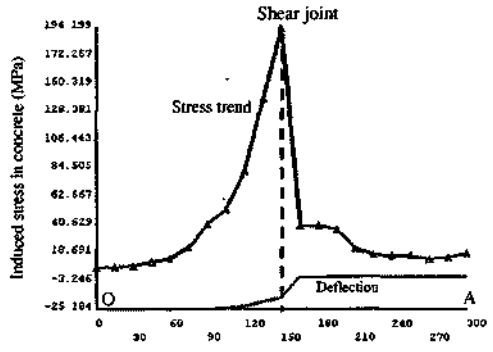

Figure 14. Yield stress trend in concrete with 40 MPa strength and thick resin without pretension effect

The rate of strain changes along the bolt, with thick resin thickness in 40 MPa concrete and without pretension, is shown in Figure 15. It was found that the outer layer of the bolt was yielded, however, the middle part of the bolt cross section remained in the elastic state in different concrete strength.

Moreover, with increasing the bolt pretension load, the area of tensile strain expanded and distributed to the middle of the bolt.

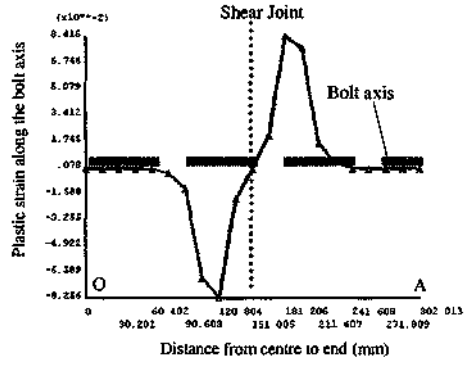

Figure 15- Trend of axial strain along the bolt in high resin thickness (5 mm) surrounded by 40 MPa concrete

4 THE EFFECT OF RESIN THICKNESS ON INDUCED STRESSES

The value of induced stresses in bolt was evaluated m different resin thickness The behaviour of the concrete and grout were assumed as an isotropic linear material and the behaviour of steel bolt was assumed non-linear hardening The effect of various concrete, grout and bolt modulus of elasticity m different resin thickness was investigated using the numerical simulations Shear stress trend as a function of concrete modulus in different resin thickness is shown in Figure 16 The shear stress along the bolt in thick resin layer is lower than in thin resm layer This trend was reduced with increasing concrete modulus Figure 17 displays induced tensile stress versus grout modulus in soft concrete and in different resin thickness The induced tensile stress along the bolt was decreased with increasing resm thickness and grout modulus

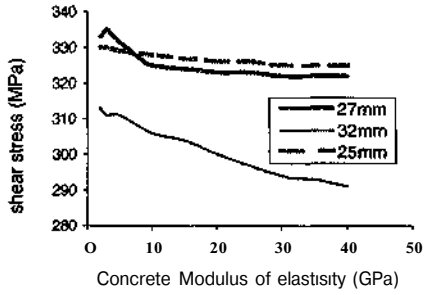

Figure 16- Induced shear stress versus concrete modulus of elasticity m different resin thickness

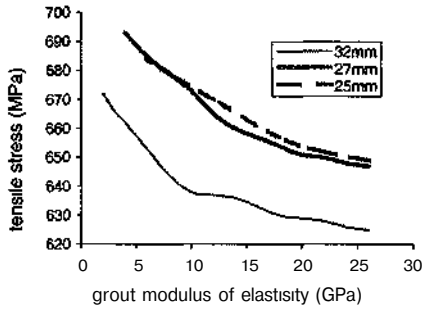

Figure 17- Induced tensile stress versus grout modulus of elasticity in soft concrete

Figure 18 shows the effect of concrete modulus on shear displacement in different resm thickness Concrete strength has great effect on shear displacement in all resm thickness However, no significant change m shear displacement in high strength concrete was observed The value of shear displacement in thin resin layer is higher than thick Iayei As Figure 19 shows the influence of grout modulus is more effective than the concrete modulus in shear displacement for the variety of resin thickness

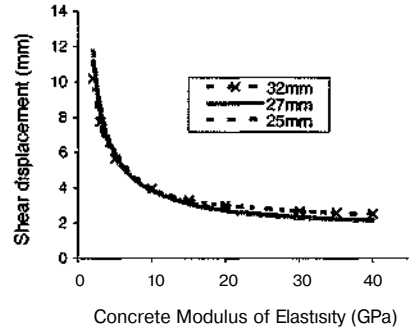

Figure 18- Shear displacement versus concrete modulus m different resm thickness

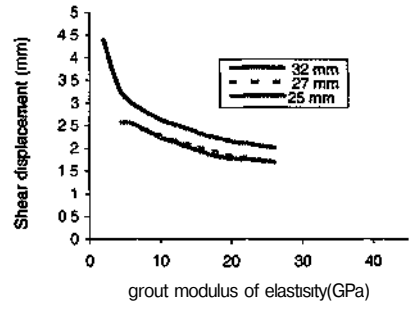

Figure 19 Shear displacement versus grout modulus of elasticity in different resin thickness

5 RESULTS AND CONCLUSION

This paper demonstrated that the resm thickness plays a prominent role in bolt shearing across joints and bedding planes Resm thickness role in shear is less significant in comparison to the conventional axial loading and load transfer characteristics What is important and influencing the bolt shear is the strength of resm in relation to the medium strength

The foilowing are some of the conclusions drawn from model simulations

- The influence of grout modulus is more effective than the concrete modulus m shear displacement for the variety of resin thickness
- Tensile and compression strains and shear displacement were slightly reduced with increasing resin thickness
- The plastic strains perpendicular to the bolt axis inside the grout were reduced with increasing resin thickness
- Compression and tensile strains along the bolt axis in concrete interface were slightly reduced with increasing resin thickness, and
- The strength of the surrounding concrete has greater influence in shear resistance, and shear displacement than the resin thickness, when bolt is loaded laterally

REFRENCESES

ANSYS (Vers 8 1) Reference Manuals 2003

Aziz, N Webb, B (2003) Load transfer Appraisal of bolts using short encapsulation push test *4th* Underground Coal Operarors, Conference Wollongong 72-81

Aziz, N (2004) Bolt surface profiles- an important parameter in load transfer capacity appraisal Proceedings of the fifth International conference on ground control and mining construction, September, Perth pp-221-230

Aziz, N, Jalalifar H, Hadi M The effect of rock strength on shear behaviour of fully grouted bolts Fifth International Symposium on ground support in Mining and Underground Construction 28-30 September, Perth Australia, 2004 pp 243-251

Azuar JJ Stabilization de massifs rocheux fissures par barres d'acier scellées Rapport de recherché No 73 Laboratoire Central des ponts Chaussées, France

Bjurstrom S Shear strength of hard rock joints reinforced by grouted untensioned bolts Proceeding 3rd Int Conf ISRM congress, Denver, 1974 1194-1199

Dıght P Improvement to the stability of rock walls in open pit mines PhD thesis, Monash University, Victoria, Australia, 1982,282p

Dulacska H 1972 Dowel action of reinforcement crossing cracks in concrete American Concrete Institute J Proc Vol 69 No 12 pp 754-757

Fabjanczyk, M, Hurt K & Hindmarsh D (1992) Optimization of roof bolt performance 1998, Proceedings of the International Conference, Geomechanics/ground control in Mining and Underground Construction, UOW, NSW, July 413-424

Ferrero AM The shears strength of reinforced rock joints Int J Rock Mech Mm Sei & Geomech. Abstr, 1995,32, 6 595-605

Grasseli, G 3D behaviour of bolted rock joints Experimental and numerical study Int J Rock Mech &Min Sei 2004

Hıbıno S and Motojıma M Effects of rock bolting in jointed rocks Proc Int Symp Weak rock, Tokyo , 1981, 1052-1062

Hass, CJ (1981) Analysis of rock bolting to prevent shear movement m fractured ground Mining Engineering, Vol 33, pp 698-704

Jalahfar,H Azız N, Hadi M Shear behaviour of bolts in joints with increased confining pressure conditions International Mining Symposium, 2-3 June 2004, Aacken, Germany Pp 211-226

Kharchafi M, Grasselli G and Egger P 3D behaviour of bolted rock joints Experimental and Numerical study, Symposium of Mechanics of jointed and Faulted Rock, Rossmamth, Rotherdam.,1998, 299-304

Long, LJ, 1985 A simple numerical representation of fully bonded Computers and Geothecnics 79-97

Nitzsche, R N and Hass C J (1976) Installation induced stresses for grouted roof bolts Int J Rock Mechanics and Min Sei Vol 13 pp 17-24

Pellet F and Boulon M A Constitutive model for the mechanical behavior of bolted rock joint Proc Of the Int Conf On Mechanics of jointed and faulted Rock, Rossmamth, Rotherdam., 1998, 179-183

Spang K and Egger P Action of fully Grouted bolts in jointed rock and factors of influence Rock Mechanics and Rock Engineering, 1990,23 201-229

Swoboda G and Marence M Numerical modeling of rock bolts m intersection with fault system Numerical models in Geomechamcs , 1992, 729-737

The 19th International Mining Congress and Fair of Turkey, IMCEV2005, İzmir, Turkey, June 09-12, 2005

Interaction Between Parallel Underground Openings

H. Gerçek
Department of Mining Engineering, Zonguldak Karaelmas University, Zonguldak, Turkey

ABSTRACT: The paper involves a parametric study for investigating the interaction between parallel underground openings that have conventional shapes. The parameters of the study are related to problem geometry and in situ stress conditions. For this purpose, a two-dimensional finite element program with elasto-plastic stress analysis capability is used. The effects of size and relative position of openings on the interaction are investigated. The openings are located in a hydrostatic or an anisotropic in situ stress field. The results indicate that almost all the parameters studied affect the interaction of parallel openings in one way or another.

1 INTRODUCTION

Interaction between underground openings is one of the complex problems that a mining engineer encounters in the design of mine excavations. In many cases, the interaction among the mine openings is three dimensional and three-dimensional methods are required for studying such situations accurately. Yet, in some instances, when the longitudinal axes of openings are parallel to each other and also to one of the principal components of in situ stress field, the interaction problem becomes two dimensional and, then, a much simpler plane- strain analysis may be sufficient, to analyze it. In fact, a number of researchers have investigated the distribution of stresses around parallel underground openings by two-dimensional elastic - stress analyses. Unfortunately, available closed-form solutions involve only circular openings, and the opening shapes commonly employed in mining, therefore, can only be studied by numerical stress analysis.

In this study, some important aspects of the interaction phenomenon occurring between closely located and unsupported parallel underground openings are investigated. „Firstly, the approaches commonly employed for siting of parallel tunnels or underground galleries are summarized. Then, secondly, the mathematical or closed-form solutions available for the stresses around parallel tunnels are reviewed. Thirdly, important features of a parametric study for the analysis of interaction problem are described. Finally, the significant results of the study are presented and their implications are discussed.

2 SITING OF PARALLEL OPENINGS

Bieniawski (1984) considers the interaction between adjacent openings as one of the principal factors affecting stability of mines and tunnels. Therefore, in the design of parallel underground openings excavated close to each other, the effect their interaction on the overall stability should be taken into consideration. Siting of parallel underground galleries is sometimes a formidable task for mining engineers. For instance, deciding on the degree of allowable interaction between the openings and determining the size of a safe pillar between the neighboring openings are among the interesting problems of rock engineering.

Of course, there are always rules of thumb for practicing engineers. For example, according to US Army Corps of Engineers (1978), when two or more parallel tunnels are planned, the minimum width of a pillar to be left between unsupported tunnels should be 1 to 1.3 tunnel diameters in competent rock and 3 diameters or more in poor quality rock masses.

In addition, there are theoretically more reliable approaches. In this respect, the concept of "the zone of influence of an excavation" proposed by Bray (1987) has been very useful. When an underground opening is excavated, the in situ stress field is disturbed in such a way that the disturbance is largest in the close proximity of the opening and it diminishes rapidly away from the opening. The region surrounding the opening within which the disturbance is significant is called as "the zone of influence" (Bray 1987). The dimensions of the zone of influence depend on opening geometry (i.e. size and shape) and in situ stresses. This concept can be

used for siting two or more excavations in close proximity. If none of the zones of influence overlap each other, the interaction between the excavations is virtually negligible. As a matter of fact, the excavations of which boundaries are located outside of one another's zones of influence can be designed by ignoring the presence of all others (Brady & Brown 1993). Using closed-form elastic solutions for stresses, Bray (1987) derived and presented practical expressions for determining the width and height of the zone of influence for circular and elliptical openings. According to these expressions, in a hydrostatic stress field, the mechanical interaction between two circular openings of the same size can be considered insignificant if the width of pillar left between them is greater than two tunnel diameters. Similar findings were reported by Ohaboussi & Ranken (1977), who studied the interaction between two parallel circular tunnels by finite element analyses.

3 STRESSES AROUND PARALLEL UNDERGROUND OPENINGS

Jeffrey (1920) was the first researcher who developed plane elasticity equations in bipolar coordinates and a stress function applicable to the problem involving an infinite plate with two circular holes. Although he did not present a solution for this case, it was the first theoretical approach applicable to the problem of parallel tunnels, and a number of others followed it.

Howland (1935) investigated the stress distribution around an infinite row of equal size circular holes spaced equally in an infinite elastic plate. The plate was subjected to a uniaxial stress field (either parallel or perpendicular to the line of holes). By using principle of superposition, solution for biaxial stress fields can be obtained for this problem. Howland & Knight (1939) presented stress functions for the problems involving equal size circular holes (e.g. one or two pairs, a single row or double rows, etc.). However, no explicit solution was given for the particular cases considered.

In 1948, Ling developed a widely referenced solution (in bipolar coordinates) for the stresses in a plate containing two equal circular holes with a variable distance between them. He considered three stress fields: uniaxial stress parallel and perpendicular to the line of centers and equal stresses in all directions. About two decades later, Haddon (1967), using the conformai mapping and complex variable techniques, presented a solution for stresses around two unequal circular holes in an infinite plate. The plate was subjected to a uniaxial stress field with a variable inclination to the line of centers. This interesting solution, though tractable, involves too many terms and coefficients.

More recently, Gerçek (1988, 1996) presented a solution for boundary stresses for two parallel circular tunnels located in a biaxial in situ stress field. It was obtained by superposing the solutions developed by Ling (1948). In addition, Zimmerman (1988, 1991) gave approximate expressions for stress concentrations in an infinite elastic plate containing two circular holes.

Although the solutions mentioned above are not exhaustive, all the available closed-form solutions involve only elastic behavior and circular openings; for that reason, the openings with conventional shapes and excavated in elasto-plastic rock masses can only be studied by numerical stress analysis. In the following sections, a summary of such a study is presented.

4 STRESS AND STABILITY ANALYSES

The important aspects of the stress and stability analyses are summarized below.

4.1 Numerical Stress Analysis Program

In the study, Phase^2 computer program is employed for the stability analysis of parallel underground openings. Phase^2 (v5.0) is a two-dimensional elasto-plastic finite element program for calculating stresses and displacements around underground or surface excavations (Rocscience 2004). It can be used for studying and geomechanical evaluation of a wide range of mining and civil engineering projects (e.g. complex underground mining excavations or tunneling problems, surface excavations such as open pit mines, and slopes in rock or soil). The program is well suited for parametric studies because of its friendly capability for creating models (including automatic mesh generation and refinement), efficiency in performing nonlinear stress analysis, and versatility in interpreting results with interface tools. Further information about Phase^2 can be found elsewhere (Rocscience 2004).

4.2 Problem Geometry

The problem geometry is depicted in Figure 1. It involves two parallel underground openings. They are of conventional shape having an ached roof and a flat floor. The width-to-height ratios of the openings are Wi/Hi and W2/H2. The minimum width of the pillar left between the openings is W_P. The angle a characterizes the orientation of the openings with respect to each other. In the study the following parameters are considered: W1/H1 = W_2/H_2 = 2; $W,/W_2$ = 1 and 2; $WrWi$ =0.5; a = 0, n/4, and n/2.

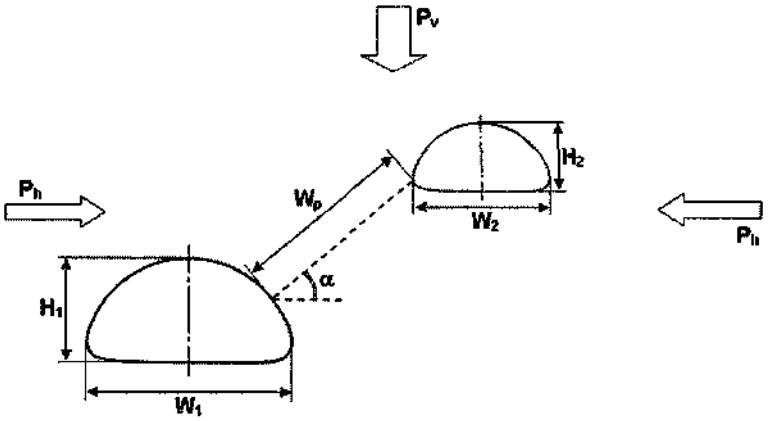

Figure 1. Geometrical parameters and in situ stress field considered in the numerical analyses.

4.3 Rock Mass Properties

In the analyses, the rock mass behavior is assumed to be elasto-plastic. For the characterization of rock mass strength, the following version of the Hoek-Brown empirical failure criterion (Hoek & Brown 1997) is considered:

$$\sigma_1' = \sigma_3' + \sigma_{ci} (m_b \sigma_3' / \sigma_{ci} + s)^{0.5} \quad [1]$$

where oV and o_3' are the maximum and minimum principal effective stresses, respectively, at failure, and Od is the uniaxial compressive strength of intact rock. The Hoek-Brown constants m_b and s depend on the quality of the rock mass, and they can be estimated by the following empirical expressions involving the Geological Strength Index (Hoek & Brown 1997) or GSI:

$$m_b = m_i \exp[(GSI-100)/28)] \quad [2.a]$$

$$s = \exp[(GSI-100)/9)] \quad [2.b]$$

where mi is the material constant for intact rock. In the numerical analyses, the following strength parameters have been used for the intact rock material: mi = 10 and a^ = 75 MPa. Also, the following Hoek-Brown strength parameters have been used for the original rock mass: GSI = 70, m_b = 3.43, and s = 0.036.

For the failed rock mass, the following expressions suggested by Ribacchi (2000) are used.

$$m_r = 0.65 \text{ mi}, \quad [3.a]$$

$$s_r = 0.04 \text{ s} \quad [3.b]$$

Then, the strength parameters are m_r = 2.23 and s_r = 0.00143 and the dilatation parameter is assumed to be zero.

The deformation modulus of the rock mass is estimated by the following empirical expression suggested by Hoek & Brown (1997):

$$E_m (GPa) = [\sigma_{ci} (MPa) / 100]^{0.5} \, 10^{(GSI-10)/40} \quad [4]$$

Thus, the elastic properties for the rock mass are as follows: E_m = 27.4 GPa, v (Poisson's ratio) = 0.25.

4.4 In **Situ** Stress **Field**

The results of numerous in situ stress measurements carried out at various regions of the world indicate that, unless there is any significant geological effect, the principal in situ stresses do not deviate very much from the vertical and horizontal directions (Amadei & Stephansson 1997). In the study, too, it is assumed that the principal components of the in situ stress field act in vertical, horizontal, and axial (longitudinal) directions with respect to the parallel openings, and they are P_v, P_b, and P_z, respectively (Fig. 1).

In addition, both isotropic (ı e hydrostatic) and anisotropic in situ stress fields have been considered in the numerical analyses

4 4 1 *W opıc in situ stresses*

Consideration of hydrostatic m situ stress field m the stress and stability analyses of underground openings facilitates solutions and interpretation of results For a circular opening, if failure occurs, the thickness of failure zone is expected to be constant m a hydrostatic stress field In addition, it has long been recognized that if failure occurs around a non-circular underground opening located m a hydrostatic in situ stress field, the thickness of failure zone is larger at the parts of boundary where the radius of curvature is larger or vice versa

In the study, the hydrostatic in situ stress is taken as $P_v = P_h = P_z = P_0 = 20$ MPa to cause a substantial zone of failure around the openings According to the closed form solution of Brown et al (1984) for a circular tunnel excavated m a rock mass with given strength parameters and $P_0 = 20$ MPa, the thickness of the failure zone is about 14 5 % of the tunnel diameter

4 4 2 *Anisotropic in situ stresses*

The in situ stress measurements reported in the literature also indicate that the magnitudes and order of principal components are quite variable (Amadei & Stephansson 1997) In fact, anisotropic in situ stress field is a common occurrence throughout the world

In this study, in order to impose a considerable anisotropy for the in situ stress field, its major, intermediate, and minor principal components are chosen as Pi = 30 MPa, $P_2 = 20$ MPa, and $P_3 = 10$ MPa, respectively The anisotropic m situ stress combinations considered in the analyses are given in Table 1

Table 1 The anisotropic in situ stress combinations considered in the study

Case	P, (MPa)	Ph(MPa)	**P_1(MPa)**	**k = P_v/P_h**
Al	10	20	**30**	**2 0**
A2	10	30	**20**	**3 0**
A3	20	**10**	**30**	**0 5**
A4	20	30	**10**	**1 5**

These in situ stress states represent equivalent stress points with respect to the the Hoek-Brown yield surface In other words, in the principal in situ stress space, the stress points are on the same octahedral plane (Eqn 5a), they are located at equal distances from the hydrostatic stress axis (Eqn 5b), and they represent pure shear (Eqn 5c) Then the following expressions can be given for these stress points

$$I_1 = P_v + P_h + P_z = 60 \text{ MPa} \quad [5a]$$

$$J_2^{1/2} = \{[(P_v-P_h)^2+(P_h-P_z)^2+(P_z-P_v)^2]/6\}^{1/2} = 10 \text{ MPa} \quad [5b]$$

$$\theta = \{\arcsin [-1.5 J_3 (3 / J_2^3)^{1/2}]\} / 3 = 0 \quad [5c]$$

where I_1 = first invariant of the m situ stress tensor, J2 and J3 = second and third invariants, respectively, of the deviatonc m situ stress tensor, and 0 = Lode angle

4 5 Evaluation of Stability

The results of a stress analysis may be evaluated in many ways, e g by looking at the distribution of pnncipal components of induced stresses or displacements occurring around the openings One of the more meaningful approaches is to evaluate the distribution of local safety factors around the underground openings along with the failure zones if they develop This is an indication of how the excavations change the stability picture withm the immediate neighborhood of the openings Also, in comparison of situations with different m situ stress fields, one should be very careful since the results may be misleading if the initial conditions (1 e m situ stress states) are not equivalent

5 RESULTS OF THE ANALYSES

In this section, significant results of the numerical analyses are presented, firstly, for the hydrostatic in situ stress field and, then, for the anisotropic in situ stress cases

5 1 Isotropic In Situ Stresses

Before studying the interaction problem, the stability picture of a single isolated opening has been determined for hydrostatic in situ stresses For this purpose, the distribution of safety factors around the opening and the size of failure zone are examined (Fig 2a) Then, the effect of pillar width (W_p) on the interaction between two parallel openings of the same size (1 e $W_1 = W_2$) is investigated for the same in situ stresses The cases with W_p/W_i =0 5, 1, and 15 are considered (Figs 2b, 2c, and 2 d, respectively) As expected, for the opening shapes considered, practically no interaction exists between the parallel openings when $W_p/W_i > 1$ 5 (compare Figs 2a and 2d) Also, it is noted that the interaction is minimal when $W_p/W_i = 1$ In order to study the interaction more closely, the pillar width is taken as one-half of the opening width (1 e $W_p/W_i = 0$ 5) for the remainder of the study

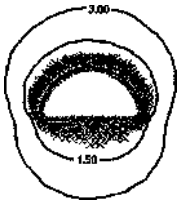

a. Single isolated opening.

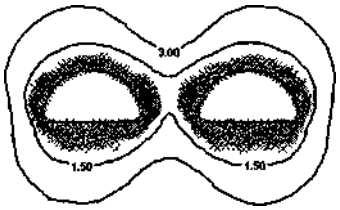

b. Parallel openings with W_P / W, = 0.5.

c. Parallel openings with W_P/ W, = 1.

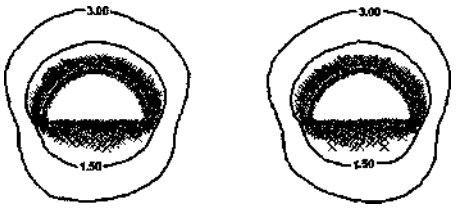

d. Parallel openings with W_P / Wj = 1.5.

Figure 2. Effect of the pillar width on the degree of interaction.

Then, the effect of the position of openings with respect to each other is examined. Three different alignments of openings are considered: horizontal alignment (a = 0), diagonal alignment (a = n/4), and vertical alignment (a = *nil).* The distribution of safety factors and the failure zones are illustrated in Figure 3. It is noted that, for such a close siting, the vertical alignment of openings is the worst position in terms of stability; actually, this is to be expected since the parts of opening boundaries with larger radius of curvature are opposite to one another.Also, for the hydrostatic in situ stress field, the interaction between parallel openings with different sizes is studied. The dimensions of one of the openings is taken as one-half of those of the other (i.e. Wi/W_2 = 2). In this respect, the same (i.e. horizontal diagonal, and vertical) alignments apply with one dih.rence. There are two versions of the vertical alignment: the smaller opening is situated just above (a = Jt/2) or just below (a = -it/2) the larger one. In all cases, the width of pillar between the openings is taken as equal to the width of smaller opening (W_P = W2). The results of the analyses are depicted in Figures 4a to4d.

a. Horizontal alignment (a = 0).

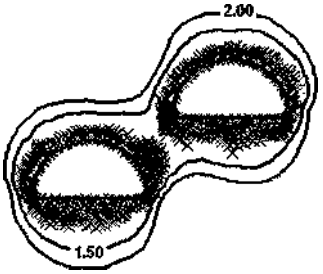

b. Diagonal alignment (a = 7t/4).

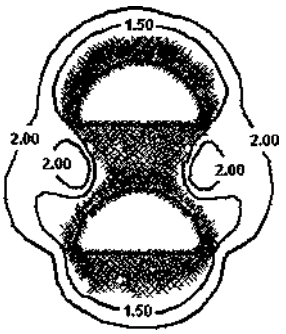

c. Vertical alignment (a = *itfl).*

Figure 3. The effect of positions of openings on the interaction in a hydrostatic in situ stress field.

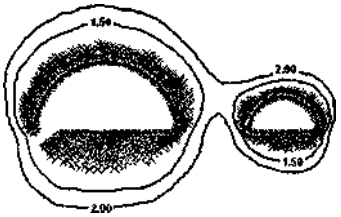

a. Horizontal alignment (a = 0).

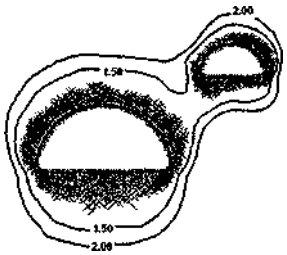

b. Diagonal alignment (a = *n* /4).

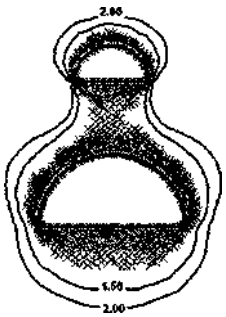

c. Vertical alignment (ot = *n 12).*

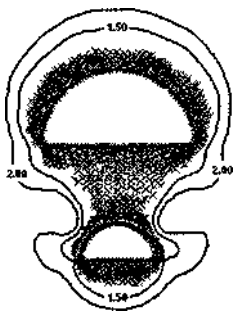

d. Vertical alignment (a = - *n 11).*

Figure 4. Interaction between openings with different sizes in a hydrostatic in situ stress field.

Similar to the situation with openings of equal size, in the cases involving excavations with different sizes, the vertical alignment positions (Figs. 4c and 4d) result in worse stability conditions than those of the other cases. Again, in these cases, the parts of opening boundaries with larger radius of curvature are opposite to one another and, therefore, almost the entire section of the pillar left between the openings is subjected to high stresses.

5.2 Anisotropic In Situ Stresses

Similarly, stability of a single isolated opening has been determined for the anisotropic in situ stress cases given in Table 1. Contours of safety factor and failed regions around the single openings are determined. The results of Cases Al and A2 (i.e. P_v is the minimum component of the in situ stresses) are shown in Figure 6 while the results of Cases A3 and A4 (i.e. Pv is the intermediate component of the in situ stresses) are shown in Figure 7.

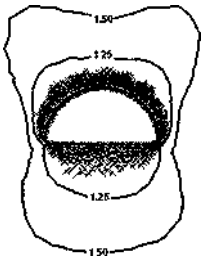

a. Case Al (P_v = 10 MPa, P_h = 20 MPa, P_z = 30 MPa).

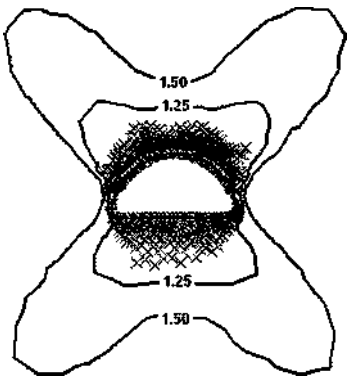

b. Case A2 (P_v = 10 MPa, P_h = 30 MPa, P_2 = 20 MPa).

Figure 5. Contours of safety factor and failed regions around the single openings when P_v is the minimum component.

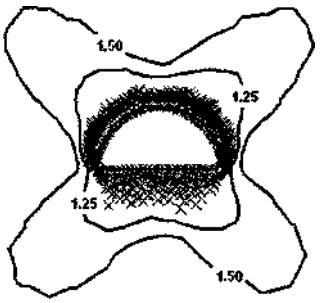

a. Case A3 (P, = 20 MPa, P_h = 10 MPa, P_2 = 30 MPa).

b. Case A4 (P_v = 20 MPa, P_h = 30 MPa, P_2 = 10 MPa).

Figure 6. Contours of safety factor and failed regions around the single openings when P_v is the intermediate component.

According to these initial analyses, when P_V is the minimum in situ stress component, orienting the opening parallel to the larger of the horizontal stresses (i.e. Case A1) results in considerable smaller yield or overstressed region, compared to me reverse situation (Fig. 5). This is in agreement with the recommendations and reported cases encountered in the literature. However, when P_v is the intermediate in situ stress component, somewhat opposite results have been obtained. In this case, orienting the opening parallel to the smaller of the horizontal stresses (i.e. Case A4) has resulted in significant decrease in the size of overstressed region (Fig. 6). Similar findings were also reported by Gerçek & Genis (1999).

The implication of these phenomena for the interaction problem is that any in situ stress condition or opening orientation which is unfavorable for a single opening will also be undesirable for closely spaced parallel openings. Indeed, the outcome of analyses involving anisotropic in situ stresses has confirmed the findings. For that reason, when P_v is the minimum component, only Case Al is shown in Figure 7 since Case A2 is already known to be worse in terms of stability. Among the three different positions, again, the vertical alignment of openings is the most unfavorable one (Figs. 7a-c).

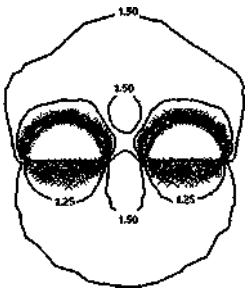

a. Horizontal alignment (a = 0).

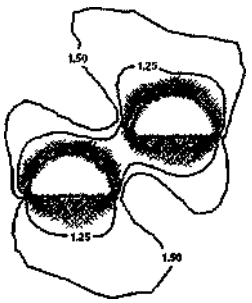

b. Diagonal alignment (a = 3t/4).

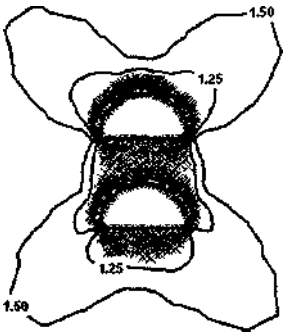

c. Vertical alignment (a = n/2).

Figure 7. Interaction between openings in an anisotropic in situ stress field (Case A1; P_v = 10 MPa, P_h = 20 MPa, P_z = 30 MPa).

Finally, the other anisotropic in situ stress conditions, in which P_v is the intermediate component, (i.e. Cases A3 and A4) are considered. In terms of stability, Case A3 is worse than Case A4. In Figure 8, results of the analyses for parallel openings with different sizes are shown for Case A3. It is interesting to note that, as regards to stability, the diagonal alignment of openings is the least desirable one (Figs. 8a-c).

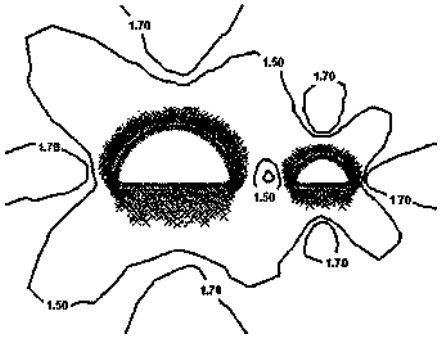

a. Horizontal alignment (a = 0).

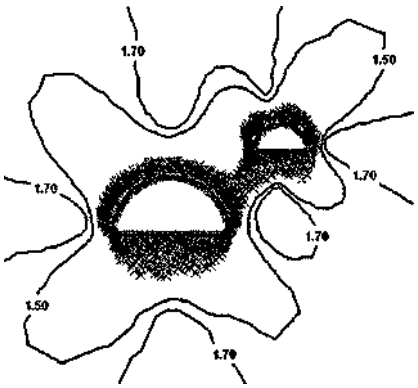

b. Diagonal alignment (a = 7t/4).

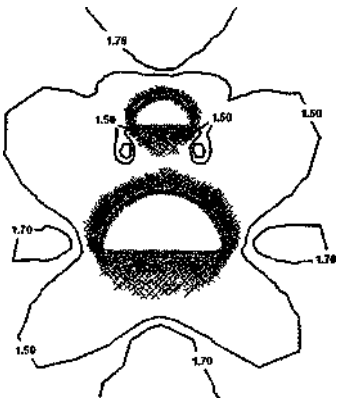

c. Vertical alignment (a = *TU2).*

Figure 8. Interaction between openings in an anisotropic in situ stress field (Case A3; P, = 20 MPa, P_h = 10MPa, P_z = 30MPa).

6 CONCLUSION

Interaction between closely spaced and parallel underground openings with complicated geometry can be studied by only numerical stress analysis. In addition to the in situ stresses field, the geometry (size and shape) of openings and their position with respect to each other are important factors that affect the degree of interaction.

REFERENCES

Amadei, B. & Stephansson, O. 1997. *Rock Stress and its Measurement.* Chapman & Hall, London.

Bieniawski, Z.T. 1984. Rock *Mechanics Design in Mining and Tunneling,* A.A. Balkema, Rotterdam.

Brady, B.H.G. & Brown, E.T. 1993. *Rock Mechanics for Underground Mining,* George Allen & Unwin, London.

Bray, J:W. 1987. Chapter 2: Some applications of elastic theory. *Analytical and Computational Methods in Engineering Rock Mechanics,* E.T. Brown (ed.), Allen & Unwin, London, pp. 32-94.

Brown, E.T., Bray, J.W., Ladanyi, B. and Hoek, E. 1984. Ground response curves for rock tunnels. *J. Geotech. Engineering, ASCE,* 109 (1): 15-39.

Gerçek, H. 1988. Interaction of parallel tunnels or roadways (in Turkish). *Madencilik,* 27 (1): 39-49.

Gerçek, H. 1996. Special elastic solutions for underground openings. *Milestones in Rock Engineering - The Bieniawski Jubilee Collection,* Balkema, Rotterdam, pp. 275-290.

Gerçek, H. & Geniş, M. 1999. Effect of anisotropic in situ stresses on the stability of underground openings. *Proc. of the Ninth Intl. Congress on Rock Mechanics,* ISRM, Balkema, Rotterdam, 1: 367-370.

Ghaboussi, J. & Ranken, R.E, 1977. Interaction between two parallel tunnels. *International Journal for Numerical and Analytical Methods in Geomechanics,* 1:75-103.

Haddon, A.W. 1967. Stresses in an infinite plate with two unequal circular holes. *Quart. J. Mech. & Applied Math.,* 20: 277-291.

Hoek, E. and Brown, E.T. 1997. Practical estimates of rock mass strength. *Int. J. Rock Mech. & Min. Sei.,* 34 (8): 1165-1186.

Howland, R.C.J. 1935. Stresses in a plate containing an infinite row of holes. *Proc. Royal Soc. (Series A),* 148: 471-491.

Howland, R.C.J. & Knight, R.C. 1939. Stres functions for a plate containing groups of circular holes. *Phil. Trans. Royal Soc. (Series A),* 238: 357-392.

Jeffrey, G.B. 1920. Plane stress and plane strain in bipolar coordinates. *Trans. Royal Soc. (Section A),* 221: 265-293.

Ling, C.B. 1948. On stresses in a plate containing two circular holes. / *Appl. Physics,* 19: 77-82.

Ribacchi, R. 2000. Mechanical tests on pervasively jointed rock material. *Rock Mech. Rock Eng.,* 33 (4): 243-266.

Rocscience 2004. Phase2 v5.0, http://www.rocscience.com/products/Phase2.asp

US Army Corps of Engineers 1978. *Tunnels and Shafts in Rock* Engineer Manual, EM 1110-2-2901, Dept. of the Army, Corps of Engineers, Washington, DC.

Zimmerman, R.W. 1988. Stress concentration around a pair of circular holes in a hydrostatically stressed elastic sheet. *Journal of Applied Mechanics,* 55: 487-488.

Zimmerman, R.W. 1991. Approximate expressions for stress concentrations in elastic solids containing multiple holes or inclusions. *Recent Developments in Elasticity,* Appl. Mech. Div. - Vol. 124, ASME, New York, pp. 71-75.

Evaluation of the Relationships between Schmidt Hardness Rebound Number and Other (Engineering) Properties of Rocks

A. Güney
Muğla University, Faculty of Engineering, Department of Mining Engineering 48000 Muğla

R. Altındağ, H. Yavuz & S. Saraç
SDU, Faculty of Engineering and Architecture, Department of Mining Engineering, 32260 İsparta

ABSTRACT: This study aims to investigate the relationships between the Schmidt hardness rebound number (N) and certain engineering properties of rocks by evaluating the results obtained from two different Schmidt hammers and three different test procedures.

In the scope of this research, numerous rock samples were collected from various locations in Turkey and laboratory experiments were implemented in order to determine certain mechanical and physical properties of rocks such as uniaxial compressive strength (UCS), bending strength (BS), point load strength index (Is^o;), shore hardness (SH) and P-wave velocity *(Vp)*. The models of Schmidt hammers (N-type and L-type) were employed in the experiments for the comparison of the respective results obtained by three different assessment methods. Later, the statistical correlations were established by regression analyses to evaluate the relationships between Schmidt hardness rebound numbers and other parameters such as UCS, BS, Is5o> SH and *Vp* for each rock type, yielding high correlation coefficients.

1 INTRODUCTION

Hardness is known to be one of the physical properties of materials. Various methods to determine the hardness have been proposed (Brinell, Vickers, Rockwell, Knoop, Schmidt, Shore, Mohs) depending on the properties' of the material to be tested. In this study, hardness of the rocks was determined by N-type and L-type Schmidt hammers.

The Schmidt hammer, which was orginally developed for measuring the strength of hardened concrete (Schmidt, 1951) has later been improved to predict the strength of rocks. The Schmidt hardness test is also quick, cheap and nondestructive. In rock engineering, it is widely used for its simplicity, portability and the capability of instant data production. Today, eventough variety of Schmidt hammers are available for use, the models of L-type and N-type are extensively employed.

Presently, Schmidt hammer can be used to predict the uniaxial compressive strength of rocks, the performances of tunnel boring machines (TBM), advance speed of drilling machines as well as the evaluation of discontinuities in rock formations. Krupa et al. (1993), have developed a relationship between the specific energy W (MJ/m^3) and Schmidt hammer rebound number (N), W=0.29Af + 61.3, with a correlation coefficient of r=0.45 between the specific energy measured during the operation of full face tunnel boring machine - Wirth TB 11-330 H - in andésite and the data of hardness measurements on the walls of the same tunnel by N-type Schmidt hammer.

Young and Fowell (1978) monitored the performance of Dosco MKII-A roadheader used on mudstone in the UK and they pointed out that in fractured rock formations the primary influence on the performance of the machines were rock discontinuities characteristics rather than the intact material properties and the Schmidt hammer rebound value was a good indicator of rock discontinuity. Similar results were observed by Poole and Farmer (1980).

Numerous empirical relationships between Schmidt hammer rebound number and other mechanical and physical properties of rocks have been published in literature. A list of the some relationships proposed to predict UCS of rocks is presented in Table 1.

Table 1 Some correlations between Schmidt hardness rebound number (N) and uniaxial compressive strength (UCS) in literature

Equations	Correlation Coefficient (r)	Literature
ucs = io$^{(000014\wedge+316)}$	0 94	Deere and Miller (1966)
UCS = 6 9 n 0$^{t134W+316]}$	-	Aufmuth(1973)
UCS = 12 74 exp(0 185YA0	—	Beverly et al (1979)
UCS = 0 447 exp[0 045(/V+3 5)+ y)	—	Kıdybınskı (1980)
UCS = *2N*	0 72	Singh et al (1983)
UCS = 04AM 6	0 94	Shoeryetal (1984)
UCS = 0 *99N* 0 383	07	Haramy and DeMarco (1985)
UCS = 0 88AM 2 11	0 87	Ghose and Chakraborti (1986)
UCS = 702AM104	0 77	0'Rourke(1989)
UCS = (AM5 7244)/0 239	0 96	Sachpazis(1990)
UCS = exp(a/V+b)	0 88	Xuetal (1990)
ucs^oooi/v$^{320\wedge}$	0 84	Gokçeoğlu(1996)
UCS = 4 5*10^{-4} *(NY)*^{2} 4fi	0 93	Kahraman (1996)
UCS = exp(0 818+0 059AO	—	Katzetal (2000)
UCS = exp(0 818+0 *059N)*	0 98	Yılmaz and Sendir (2002)
UCS = 2917 2In(AO-11098	0 88	Yaşar and Erdoğan (2002)
UCS = 2 7537/V-36 826	0 97	Dmçeretal (2003)
UCS = 4 72/V$^{\circ 69}$	081	Başarır et al (2004)
UCS = 4 124AM 34 33	091	This study

N Schmidt hardness rebound number, y Density, a,b Constants,

2 LABORATORY STUDIES

Rock blocks were collected from various locations in Turkey as shown in Table 2 Seven different rock types of metamorphic and sedimentary origins were selected to conduct the Schmidt tests on cubic samples dimensioned to be 100x100x100 mm The data obtained from N-type and L-type Schmidt hammers were assessed by the methods proposed by Poole-Farmer (1980), Hucka (1965) and ISRM (1981) on these blocks All the tests were carried out with the hammer held vertically downwards and at right angels to horizontal faces of large rock blocks Therefore, a total of six different evaluation combinations were constituted for each rock type

Other rock properties studied here (compressive strength, bending strength, P-wave velocity, point load strength index and Shore hardness) were determined in compliance with the ISRM (1981), TS699 (1987) and ASTM standards as illustrated in Table 3

The tests were performed by an N type Schmidt hammer with an impact energy of 2 207 Nm, and L-type Schmidt hammer, with an impact energy of 0 735 Nm Following three of widely accepted test procedures with different Schmidt hammer rebound techniques were selected and applied on rock samples

Test Procedure 1 Poole and Farmer (1980) suggested that the peak value from at least five continuous impacts at a point should be selected

Test Procedure 2 Hucka (1965) recommended that the peak value from at least ten continuous impact at a point should be selected

Test procedure 3 ISRM (1981) suggested that twenty rebound values from single impacts separated by at least a plunger diameter should be recorded and the upper ten values averaged

Each testing method was repeated at least three times on any rock type and the average value was recorded as the rebound number The results are displayed in Table 4

Table 2 Name and location of rocks collected

Rock Code Number	Rock Type	Rock Class	Location
1	Limestone	Sedimentary	Burdur
2	Travertine	Sedimentary	Konya
3	Limestone	Sedimentary	Bilecik
4	Limestone	Sedimentary	Burdur- Karamanlı
5	Limestone	Sedimentary	Antalya-Fınıke
6	Limestone	Sedimentary	Burdur-Yeşilova
7	Marble	Metamorphic	Muğla

Table 3 Some of the mechanical properties of rocks tested

Rock Code Number	$I_{S(50)}$ (MPa)	UCS (MPa)	BS (MPa)	SH	*Vp* (m/s)
1	4 54	138 21	176 46	64 62	6007
2	52	58 81	129 28	45 62	5383
3	5 12	92 6	173 91	59 85	6124
4	62	110 24	173 84	62 44	6188
5	3 07	52 49	123 18	33	4636
6	4 24	13191	177 63	62 25	5979
7	4 05	48 71	124 33	42 21	5789

Table 4 Schmidt hardness test results

Rock Code Number	L-Type			N-Type		
	Test Procedure 1	Test Procedure 2	Test Procedure 3	Test Procedure 1	Test Procedure 2	Test Procedure 3
1	55	56	57 5	60	60 67	603
2	46 33	48 67	45 7	50	50 33	47 9
3	61	6133	56 6	63 33	64	60 2
4	52 33	54	60	65 33	65 67	62 8
5	45	47 33	39 7	48 33	50 33	44
6	59 67	60 67	56 9	62 67	63 67	61
7	43 67	47 67	43	48	49	45 3

3 STATISTICAL ANALYSIS

In order to be able to describe the relationships between Schmidt hardness rebound number and the UCS, BS, *Vp,* (IS(50)) and SH, regression analyses were performed The equation of the best-fit line, the 95% confidence limits, and the correlation coefficient (r) were determined for each regression analysis Best fit lines for each test procedure are shown m Figures 3-8 In this work, high correlation coefficients between *N* values and other rock properties (UCS, BS, *Vp,* ($I_{s_{(50)}}$) and SH), as shown m Table 5, were established indicating that Schmidt hammer rebound number is strongly related with other mechanical and physical properties of rock materials

Table 5 Correlations between Schmidt hardness (N-type) rebound number (N) and other properties of rocks

Equations	Correlation coefficient (r)
Vp = 0 0541N+2 7796	0 817
IS(50) = 0 0739/V+0 604	0617
UCS = 4 124AM34 33	0 908
BS = 0 3117^-1 8812	0 989
SH = 1 4502W-26 182	0 971

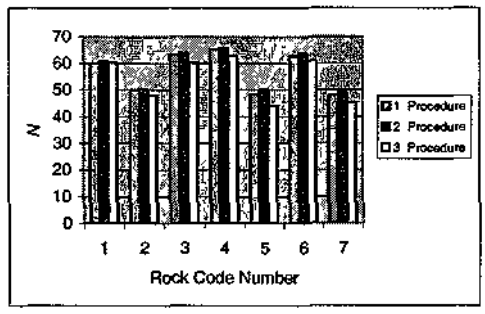

Figure I Rebound values for N-type Schmidt hammer

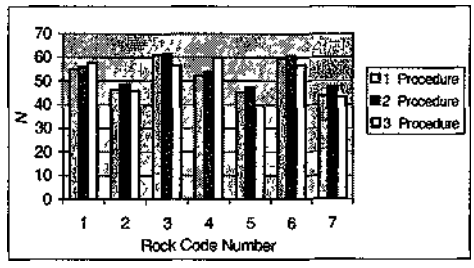

Figure 2 Rebound values for L-type Schmidt hammer

The results obtained from N-type and L-type Schmidt hammers via three different test procedures as descibed earlier were illustrated in Table 4 and then assessed in bar graphs in Figures 1 and 2, in which the hardness rebound numbers of N-type Schmidt hammer appear to be slightly higher than those of L-type Schmidt hammer. When the results of test procedures were compared, procedure 3 yielded relatively lower rebound numbers for both Schmidt hammers than that of other two test procedures, perhaps owing to differences in the application of this procedure. Thus, test procedure 3, we assume, may represent the surface hardness of rocks more reliably since measurements are conducted on at least twenty seperate points on the same sample, unlike other two procedures m which the peak value out of five or ten impacts on the same point is selected to be the Schmidt hardness of the rock tested. Besides, procedures 1 and 2 may result in higher Schmidt hardness rebound values for inelastic rocks owing to the repeated impacts on the same point, which may lead to an increase in the elasticity of the rock on the impact point and consequently induce a rmsrepresentaion on behavior of entire rock sample. Therefore, in this study, statistical analyses of the data of N-type Schmidt hammer were implemented solely by procedure 3 suggested by ISRM as depicted in Figures 4 through 8.

Relationship between Schmidt hammer rebound number and other properties of rocks resulted in reliable relationship equations with considerably high correlation coefficients as demonstrated in Table 5.

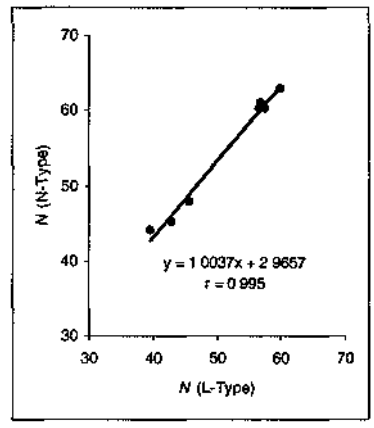

Figure 3 The relationships between Schmidt hardness rebound number *(N)* of N-type vs. L-type

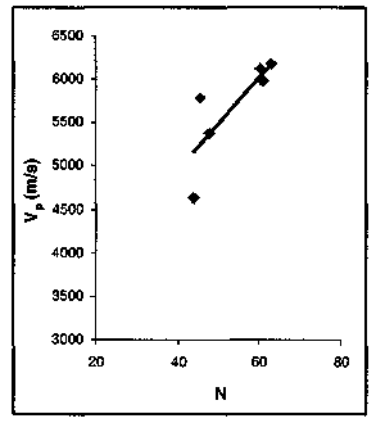

Figure 4 P-wave velocity vs Schmidt hardness rebound number (N-type)

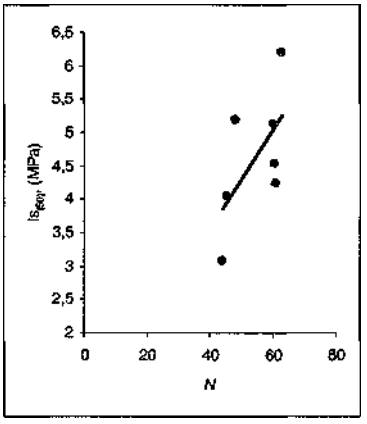

Figure 5. Point load strength index vs. Schmidt hardness rebound number (N-type).

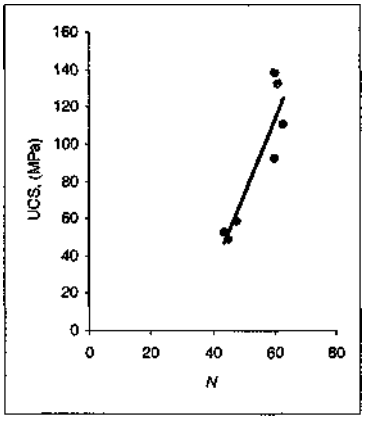

Figure 6. Corripressive strength vs. Schmidt hardness rebound number (N-type).

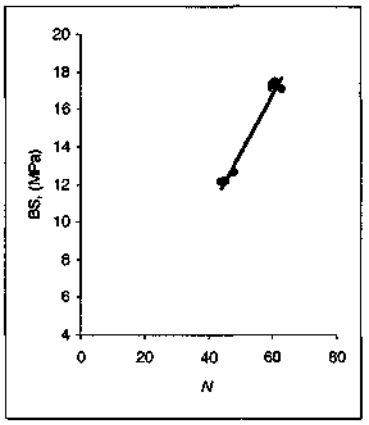

Figure 7. Bending strength vs. Schmidt hardness rebound number (N-type).

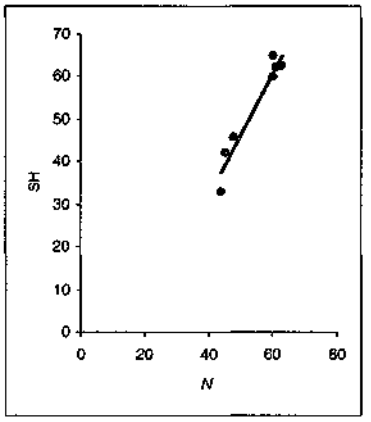

Figure 8. Shore hardness vs. Schmidt hardness rebound number (N-type).

4. RESULTS AND CONCLUSION

In this study, the data obtained by two different models of Schmidt hammers and three different test procedures were evaluated and the comparisons were made between the two models of Schmidt •hammers in addition to establishing relationships between Schmidt hammer rebound number and other mechanical and physical properties of rocks.

Experiments conducted with N-type Schmidt hammer produced slightly higher rebound numbers than those with L-type Schmidt hammer on all three test procedures However, the procedure proposed by ISRM (Test Procedure 3) yielded lower Schmidt rebound numbers than those of other two test procedures exercised m this study

Schmidt hammer, since its simplicity and capability of instant data production, has so far been a powerful tool utilized by many researchers to predict other mechanical and physical properties of rocks Although empirical relations published m literature (Table 1) do not replicate the results of the tests conducted to determine a specific rock material property Schmidt hammer rebound numbers can be correlated to other rock properties withm a reasonable error (Table 5), so that the data of Schmidt hardness tests may help designers acquire instant knowledge regarding other engineering properties of rock materials

In fact, prediction of engineering properties of rock materials e g UCS via Schmidt hardness needs to be improved to take into account more qualitative values that represent rock material better, such as the origin of the rocks, porosity, gram size and grain shape These factors affect the surface area of the interlocking bond forces at mineral gram to gram contacts In most rocks the higher the surface area of mineral gram to grain contact the harder the rock becomes The authors of this paper believe that a further study considering the factors depicted above is needed to be able to suggest more realistic empirical relations between the Schmidt hardness and other engineering properties of rocks by multi-regression analyses

REFERENCES

Aufmuth, R E, 1973, A systematic determination of engineering criteria for rocks Bull Assoc Eng Geol 11, 235- 245

Başanr.H , Kumral,M , Ozsan,A, 2004, Kayaçlarm tek eksenli basınç dayanımının basit deney yöntemleriyle tahmini, VII Bölgesel Kaya Mekaniği Sempozyumu Bildiriler Kitabı, Sivas, 111-117

Beverly, B E, Schoenwolf, D A , Bnerly, G S , 1979, Correlations of rock index values with engineering properties and the classification of intact rock

Deere, D U, Miller, R P, 1966, Engineering classification and index properties for intact rocks Tech Report Air Force Weapons Lab , New Mexico, No AFNL-TR,pp 65-116

Dmçer, I, Acar.A, Çobanoğlu, I, Uras.Y, 2003, Determination of compressive strength and average elactıcıty modulus using Schmidt hardness, (In Turkish), The Journal of Natural Science Institute, V 7, N 2, 395-401

Ghose, A K, Chakraborti, S , 1986, Empirical strength indices of Indian coals—an investigation Proceedings of 27* US Symp on Rock Mechanics Balkema, Rotterdam, pp 59-61

Gokçeoğlu, C , 1996, Schmidt sertlik çekici kullanılarak tahmin edilen tek eksenli basınç dayanımı verilerinin güvenilirliği uzenne bir değerlendirme Jeol Mühendisliği 48,78-81

Haramy, K Y , DeMarco, M J, 1985, Use of Schmidt hammer for rock and coal testing 26* US Symp on Rock Mechanics, 26-28 June, Rapid City Balkema, Rotterdam, pp 549-555

Hucka VA, 1965, A rapid method determining the strength of rocks m-situ Int J Rock Mech Mm Sei Geomech Abstr 2, 127-134

ISRM (International Society for Rock mechanics), 1981, ISRM Suggested Methods Rock Characterization Testing and Monitoring Brown ET(ed), Oxford Pergamon Press

Kahraman, S , 1996, Basınç direnci tahmininde Schmidt ve nokta yuk indeksi kullanmanın güvenilirliği in Korkmaz ve, S , Akçay, M (Eds), K T U Jeoloji Mühendisliği Bolumu 30 Yıl Sempozyumu Bildiriler Kitabı, Trabzon, pp 362- 369

Katz.O , Reches,Z, Roegıers,J C ,2000, Evaluation of mechanical rock properties using a Schmidt Hammer, Int J Rock Mech Min Sei 37, 723-728

Kıdybınskı, A, 1980, Bursting liability indices of coal Int J Rock Mech Min Sei Geomech Abstr 17, 167-171

Krupa, V Krepelka,F, Bejda, J , Imnch, P , 1993, The cutting constanat of the rock does not depend on scale effect and rock mass jointing, Scale effects in Rock Masses 93, Pinto da Cunha (Ed), 63-68

O'Rourke, J E , 1989, Rock index properties for geoengineenng in underground development Min Eng , 106- 110

Poole, R W, Farmer, I W, 1980 Consistency and repeatıbılıty of Schmidt hammer rebound data during field testing (Technical Note) Int J Rock Mech Mm Sei Geomech Abstr 17, 167-171

Sachpazis, C 1, 1990, Correlating Schmidt hardness with compressive strength and Young's modulus of carbonate rocks Bull Int Assoc Eng Geol 42, 75-83

Shorey, P R , Barat, D , Das, M N , Mukherjee, K P , Singh, B.1984, Schmidt hammer rebound data for esümatıon of large scale m-situ coal strength (Technical Note) Int J Rock Mech Mm Sei Geomech Abstr 21,39-42

Singh, R N , Hassanı, F P , Elkıngton, P A S , 1983, The application of strength and deformation index testing to the stability assessment of coal measures excavations Proc 24th US Symp On Rock Mech, Texas A&M Univ, AEG Balkema, Rotterdam, pp 599-609

TS 699, 1987, Turk Standartları Enstutusu, Tabu Yapı Taşlan - Muayene ve Deney Metodlan, p 82

Xu, S , Grasso, P, Mahtab, A, 1990, Use of Schmidt hammer for estimating mechanical properties of weak rock 6th Int IAEG Congress Balkema, Rotterdam, pp 511-519

Yaşar, E, Erdoğan, Y, 2002, Bazı kayaçlann sertlik değerlen ile fiziksel ve mekanik özelliklerinin ıstatıksel analizi, VI Bölgesel Kaya Mekaniği Sempozyumu Bildiriler Kitabı, Konya, 197-204

Yılmaz,I, Sendir, H, 2002, Correlation of Schmidt hardness with unconfined compressive strength and Young's modulus in gypsum from Sivas (Turkey), Engineering Geology, 66, 211-219

Young, R P, Fowell, R J, 1978, Assessing rock discontinuities Tunnels and tunneling, June, 45-48

The 19th International Mining Congress and Fair of Turkey, IMCET2005, İzmir, Turkey, June 09-12, 2005

Inelastic and Damage Modeling of Tunnel Face Surrounded by Discrete Elements

P.P. Prochazka
Department of Structural Mechanics, Czech Technical University, Prague, Czech Republic

ABSTRACT: The discrete elements become more and more popular in describing damage and inelastic behavior of plenty of materials. Free hexagons are used as special discrete element method to describe nucleation of cracks in soil, or rock. The problem is aimed to the stability of tunnel face. The method proposes a continuation and development of Desai's DSC (distinct state concept), which has formerly been used for saturated soils. Together with Transformation field analysis they create a powerful tool for assessment of tunnels.

1 INTRODUCTION

The neighborhood of the tunnel face is discretized into discrete elements, which are connected by fictitious springs simulating clay holding stick or causing disconnections between the elements (Prochazka 2004). The discrete elements are considered as free hexagons, their origin is in finite element method (Onck & van der Giessen 1999). Dynamical version of discrete elements can be found in (Cundall 1971), who starts with dynamical equilibrium of balls. This concept seems to be very appropriate for earthquake problems, but for almost statical problems is less advantageous. The stresses cannot be expressed, for example.

Models are considered for application to plasticity, viscoelasticity and damage in soil/rock material. Model by (Kachanov 1992) is mostly used. The method proposes a continuation and development of Desai's DSC (distinct state concept) which has formerly been used for saturated soils (Desai 1994) and extended to solid materials (Desai 1994, Moreau 1994). The extension by Desai consisted in inclusion of skeleton into the consideration and solution of such problems, which were coupled (mutual interaction of water and skeleton was studied). Prochazka and Trckova (Prochazka & Trckova 2000) introduced previously piecewise uniform eigenstrains in each material phase and precised the properties of the phases. Standard applications of the method to a two-phases rock material (stone, clay) are considered in this study, it means only one sub-volume per phase is considered. Discontinuous model is used by the discrete elements with softening respecting exclusion of tensile stress overstepping the tensile strength in springs connecting the elastic elements (Prochazka 2004). In the same time the shear cracking occurs in the tangential direction of the possible crack, which are considered in the shear springs and they make disconnections in displacements. The main disconnection is due to tensile stress in normal direction (in the springs being oriented in normal direction). In this case, the discontinuous models can be used with more promising future. Because those discrete models can describe the situation more realistic, they are worked out in more details in (Prochazka & Trckova 2001). A typical application of coupled modeling (experimental and numerical) to special case of patterns was published in (Trckova & Prochazka 2001). We hold the discontinuous model and substitute the slip caused by overstepping the damage law by introducing generalized Mohr-Coulomb law on the interfacial boundary. The different aspects of the proposed methods are systematically checked by comparing with finite element unit cell analyses, made through periodic homogenization assumptions, for three-directional lay-ups.

In order to complete the accuracy of a design of tunnel stability, Transformation field analysis (TFA) is used (Dvorak & Prochazka 1996). This is a generalization of original work by (Dvorak 1992). Another application of TFA is published in (Dvorak et al. 1999), where optimal design of bearing capacity of submersibles was solved. All the above-mentioned works on TFA are concerned with uniformly distributed eigenparameters. (Michel & Suquet 2003) ex-

tended the assumption of uniformly distributed eigenparameters to nonuniform transformation field analysis.

Starting with certain mechanical model (Desai's model in our case) the TFA brings about more accurate description of the physical conditions.

2 GENERAL CONSIDERATIONS

There are main different methods and tools that can be used to deliver the macroscopic constitutive response of heterogeneous materials from a local description of the microstructure behavior. Here we are concerned with non-linear behavior by the inelasticity of constituents or with the initiation and growth of damage. In the development of the homogenization procedures for non-linear materials we have to define both the *homogenization step* itself (from local variables to overall ones) and the often more complicated *localization step* from overall controlled quantities to the corresponding local ones.

The nonlinear problems of localization and homogenization are of a great importance today. Not only classical composites suffer from deterioration of the material due to hereditary problems (aging, viscoelasticity). On the other hand, composite materials prepared in a special way can improve properties of other material and the resulting effect can be much better than before. In this case, nonlinear and time dependent behavior has to be taken into account. From the wide scale of papers name here

The scope of the present paper is the development of constitutive equations for inelasticity and damage of heterogeneous materials that benefit from some specificities of a special boundary element method. On one hand, we need to obtain better approximations of the local stress and strain fields than in the Suquet based approaches, especially when considering damage and failure conditions. We want to simplify sufficiently the numerical techniques of overall homogenization in order to obtain a treatable system of equations that could recover the status of a constitutive equation.

The computation was run on Pentium IV PC, 2.6 GHz in FORTRAN. The program for generations of hexagonal of hexagon meshes of internal cells as well as the boundary nodes had been prepared using our own software. According to wish of the user, the meshing can be improved. The consumption of time for computation of even large system of equations, which can be stored into memory without use of hard disc or extended/expanded memory, was negligible in each step. Our illustration does not reach such dimensions of computation. It is also not necessary for such problems to increase the precision of the meshing, it losses the efficiency. The iteration at each step of loading was also very fast. It is worth noting that similar computations was carried out by the FEM, but finer meshing had to be imposed to get the comparable result with the BEM in the procedure presented. The comparison has been tested in such a way that the sum of the concentration factors should be the unit tensor.

In this contribution we are going to present the fundamental ideas of a numerical procedure leading to overall viscoelastic and damage behavior of rock matrix in a rock - tunnel lining aggregate. Based on the numerical models and mechanical laws it is possible to obtain the strain and stress in opposite to classical PFC, where no stresses are reasonably be reachable from the model (dynamical equilibrium is the starting point of balls, describing the original continuum).

Very important property of the above procedure is the non-linearity of the problem, which, when using some smart algorithm, can be solved by very powerful iterative process.

3 FREE HEXAGON ELEMENT METHOD

The free hexagon element method may be considered the discrete element method (DEM). The great disadvantage of some classical DEM, however, is the difficulty to feed them with material properties provided from laboratory tests (this is also the case of the particle flow code (PFC) (Cundall 1971), as the balls in (Cundall 1971) are connected by springs, while laboratories provide completely different material parameters being valid for continuum). This is here overcome by considering the material characteristics, which are similar to the continuum. The principal idea of classical DEM is adopted, and the domain defining the structure continuum is, in our case, covered by the hexagonal elements, and other then elastic material properties can be introduced, such as elastic-plastic, visco-elastic-plastic, etc. This step avoids the necessity to estimate the material properties of springs, which are essential, e.g. for PFC. The free hexagon element method fulfills a natural requirement due to the fact that the elastic properties are assigned to the particles, and other material parameters (angle of internal friction, shear strength, or cohesion) to the contacts of the elements. Since most particles are of the same shape it is possible to apply very powerful iteration procedures, because the stiff-

ness matrix can be stored in the internal memory of a computer.

The computational model is described in this paragraph, where the relations needed for numerical computation are also introduced. The interface conditions are formulated in the next paragraph, where the Lagrangian principle is based on the penalty method. The penalty parameters are represented by spring stiffnesses; the springs connect the adjacent elements. The material characteristics of springs can possess a large value to ensure the contact constraints. On the other hand, if, say, the tensile strength condition is violated, the spring parameters tend to zero, and in this case naturally no energy contribution in the normal direction to the element boundary appears in the energy functional. This process excludes the possibility of a multivalued solution, and uniqueness of the solution of the trial problem is ensured. If we cut out the springs when a certain interfacial condition is violated, the problem turns to singular and has not unique solution. Then the way on how the particles move in some later stages of destruction of the trial structure cannot be described.

The hexagonal particles are studied under various contact (interfacial) conditions of the grain particles (elements). In this paper two contact conditions are considered:

the generalized Mohr-Coulomb hypothesis, with exclusion of non-admissible tensile stresses along the contact (a rock mass, for example),
limit state of shear stresses and exclusion of tensile tractions along the contact (a brittle coal seam, for example).

The first case is generally connected with applications in matrices of composite materials, of shotcrete, and overburden of tunnels, etc., and the second case is more appropriate for applications in underground seams. A two-dimensional formulation and its solution have been prepared and is studied in this paper.

The problem formulated in terms of hexagonal elements (which are not necessarily mutually connected during the loading process of the body, because of nonlinearities arising due to the interfacial conditions) enables us to simulate nucleation of cracks and their propagation. The cracking of the medium can be described in such a way that the local damage may be derived. Local deterioration of the material is also shown in the pictures drawn for particular examples. Such a movement of elements and change of stresses probably cannot be obtained from continuous numerical methods.

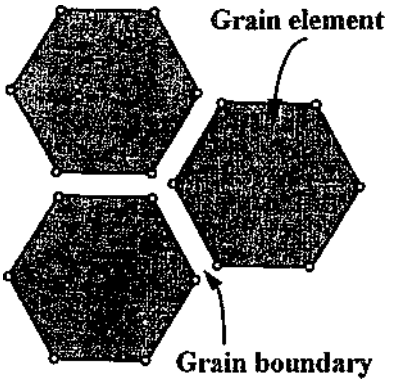

Figure 1. Geometry of adjacent hexagonal elements

3.1 Computational model

Let us now consider a single hexagonal element (described by domain Q with its boundary r). Its connection with the adjacent elements is shown in Figure 1. In each hexagonal element, the pseudo-elastic material properties are taken into consideration, i.e., in every iteration steps the element behaves linearly, but the material properties can change during the process of loading and unloading. This makes it possible to introduce only an elastic material stiffness matrix, which is homogeneous and isotropic, and we get well-known integral equations that are valid along the boundary abscissas of the hexagons, (Bittnar&Sejnoha 1996):

$$\sum_{l=1}^{2} c_{kl}(\xi)u_l(\xi) = \sum_{s=1}^{6}\left(\sum_{i=1}^{2}\left(\int_{\Gamma_s} p_i(x)u_{ik}^*(x,\xi)dx - \right.\right.$$

$$\left.\left.\int_{\Gamma_s} u_i(x)p_{ik}^*(x,\xi)dx\right) + \sum_{i=1}^{2}\int_{\Omega} b_i(x)u_{ik}^*(x,\xi)dx\right), k = 1, 2, \quad (1)$$

where b_i are components of the volume weight vector, r, are edges (abscissas) of the boundary elements, <f is the point of observation, x is the integration point, «,. are components of the vector of displacements (defined not exclusively on the boundary, but also in the domain of the hexagonal element), p_t are components of the tractions, c_u is the matrix, the values of which depend on position of

the point of observation. The quantities with an asterisk are the given kernels. The kernels can be expressed as (see (Bittnar & Sejnoha 1996), for example):

$$u^*_{ik} = A(M\delta_{ik}(\log r - \frac{\bar{x}_i \bar{x}_k}{r^2}),$$

$$p^*_{ik} = -2A\frac{\mu}{r^2}(k(n_k \bar{x}_i - n_i \bar{x}_k) - (k\delta_{ik} + \frac{2\bar{x}_i \bar{x}_k}{r^2})\bar{x}_j n_j),$$

where

$$A = -(\lambda + \mu)/4\pi\mu(\lambda + 2\mu),$$

$$M = (\lambda + 3\mu)/(\lambda + \mu),$$

$$k = \mu/(\lambda + \mu),$$

$$\bar{x}_i = x_i - \xi_i,$$

$$r^2 = \bar{x}_1^2 + \bar{x}_2^2,$$

and λ and μ are Lame's material constants.

Assuming uniform distribution of the boundary quantities (displacements $u_i(x)$ and tractions $p,(x), i = 1,2,$ and volume weight forces b_l to be uniform in the domain Ω, and positioning the points of observation ξ successively at the points x_s, which are the centers of the boundary abscissas of the hexagonal elements, a simplified version of (1) is written as:

$$\frac{1}{2}u^s_k = \sum_{s=1}^{6}(\sum_{i=1}^{2}(p^s_i \int_{\Gamma_s} u^*_{ik}(x,\xi_s)dx -$$

$$-u^s_i \int_{\Gamma_s} p^*_{ik}(x,\xi)dx) + \sum_{i=1}^{2} b_i \int_{\Omega} u^*_{ik}(x,\xi)dx), k = 1,2, \quad \textbf{(2)}$$

where u^* and p' are the values of the relevant quantities positioned at the ξ_s, s = 1,...,6, i.e., $u^s_i = u_i(\xi_s)$ and $p^s_i = p_i(\xi_s)$. Moreover, the vector of influences of the volume weight forces on the boundary abscissas is $b_s = (y,,y_2),s$= 1....6, and

$$\gamma^s_k = \sum_{i=1}^{2} b_i \int_{\Omega} u^*_{ik}(x,\xi_s)d\Gamma(x), \quad \pounds = 1,2.$$

For better and more convenient computation, the most important integrals can be calculated in advance. In this way, the integrals in (2) may be calculated directly, without numerical integration.

Let us introduce vectors a_s,ß$_s$, s = 1,...,6, and also u and p as:

$$\alpha_s = \begin{pmatrix} u^s_1 \\ u^s_2 \end{pmatrix}, \beta_s = \begin{pmatrix} p^s_1 \\ p^s_2 \end{pmatrix}, \mathbf{u} = \begin{pmatrix} \alpha_1 \\ \alpha_2 \\ \alpha_3 \\ \alpha_4 \\ \alpha_5 \\ \alpha_6 \end{pmatrix}, \mathbf{p} = \begin{pmatrix} \beta_1 \\ \beta_2 \\ \beta_3 \\ \beta_4 \\ \beta_5 \\ \beta_6 \end{pmatrix}, \mathbf{b} = \begin{pmatrix} b_1 \\ b_2 \\ b_3 \\ b_4 \\ b_5 \\ b_6 \end{pmatrix}$$

$$\alpha^s_k = \sum_{i=1}^{2}(-u^s_i \int_{\Gamma_s} p^*_{ik}(x,\xi_s)dx),$$

$$\beta^s_k = \sum_{i=1}^{2}(p^s_i \int_{\Gamma_s} u^*_{ik}(x,\xi_s)dx).$$

Using this notation, the relations on the elements (2) can be recorded as:

$$\mathrm{A\,u = B\,p + b} \quad \textbf{(3)}$$

where A and B are (12 * 12) matrices, and their components are singular integrals over the boundary abscissas. Matrix A is generally singular, while matrix B is regular. This fact enables us to rearrange equations (3) into the form:

$$\mathrm{Ku = p + V,\ \ K = B\text{-}'A, V = B\text{-}'b} \quad \textbf{(4)}$$

where the stiffness matrix K is different from that arising in applications of finite elements (here it is prevailingly non-symmetric), V is the vector of volume weight forces concentrated on the boundary abscissas (more precisely at the point ξ. In this way, the discretized problem becomes a problem similar to the FEM.

Along the adjacent boundary abscissas it should hold (p^{μ}_i are Eshelbys' forces):

$$p^+_i + p^-_i = (p^{\mu}_i)^+ + (p^{\mu}_i)^-, \quad (5)$$

where superscript plus means from the right and minus from the left (at most two particles can be in contact).

Now using the relations (4) and (5), we get twice as many unknowns as equations, because no connec-

tion between the elements has yet been introduced. Equations (5) have to be accomplished by a constraint of the type

$$k_t(u_t^- - u_t^+) = p_t. \qquad (6)$$

The latter conditions are penalty-like conditions, since if k_t is great enough, the distribution of displacements is continuous, and the displacement from the right is equal to the displacement from the left. These conditions can locally be violated, because of the contact conditions, which are discussed later in this text. Introducing boundary conditions and assuming that k_t remains great enough leads us to a stable system of equations delivering a unique solution. Even in the case when local disturbances occur, the solution can be stable. It can happen that there are too many disturbances, e.g., dense occurrence of crack, and localized damage along a path (earth slope stability violation). Then the solution is unstable, and there is a failure of the structure. This is also, for example, the case of a behavior of composites.

Discretization in the previous sense leads to a nonlinear system of algebraic equations, which are solved by an over-relaxation iterative procedure. This method is sufficient for study purposes. For a larger range of equations the conjugate gradient method has been prepared.

For displacements in the element domain $\pounds 2$ it holds:

$$u_k(\xi) = \sum_{s=1}^{6}\Big(\sum_{i=1}^{2}\Big(p_i^s\int_{\Gamma_s} u_{ik}^*(x,\xi)dx - u_i^s\int_{\Gamma_s} p_{ik}^*(x,\xi)dx\Big) + \sum_{i=1}^{2} b_i^s\int_{\Omega} u_{ik}^*(x,\xi)dx\Big), k = 1, 2, \quad (7)$$

where the element boundary displacements and tractions are known from the previous computation, providing the solution is stable. Using kinematical equations and Hooke's law, the internal stresses can be calculated from (7). There is no danger of singularities, as the points x and ξ never meet (point ξ lies inside the domain Ω and x on boundary Γ).

3.2 Formulation of the contact conditions

Recall that displacements are described by a vector function u = $<u_1,u_2>$ Jof the variable x - (x_1,x_2). The traction field on the particle boundaries is denoted either as p = (p_1,p_2), or after projections to normal and tangential directions as p = (p_n,p_t) • A similar result is valid for projections of displacements, u = (u_n,u_t). Assuming the "small deformation" theory, the essential contact conditions on the interface may be formulated as follows (no penetration conditions):

$$[u]_n^k = u_n^{k\,c} - u_n^{k\,a} \le 0 \quad \text{on} \quad \Gamma_C^k, \qquad (8)$$

where /jf, k = 1,...,« are boundaries between adjacent particles, «*" is the normal displacement of current element $a = c$ and $a = a$ belongs to the adjacent element, both on the current common boundary , r£, k runs numbers of all common sides of the particles, n is the number of common sides of hexagons (having exactly two adjacent particles inside the domain, one or none on the external boundary).

Let **t** * be the spring stiffness in the normal direction and k_n^k be the spring stiffness in the tangential direction on

the boundary between particles with a common boundary r*. Then in the elastic region $p_n^k = k_n^k[u]_n^k$ and $p_t^k = k_t^k[u]_t^k$. Denote

$$K = (u \in V, (p_n^+)^k \ge p_n^k = k_n^k[u]_n^k,$$

$$\text{if } (p_n^+)^k \le p_n^k \text{ then } p_n^k = 0,$$

$$k_t^k|[u]_t^k| \le c^k \quad \text{on} \quad \Gamma_C^k, \quad k = 1,\ldots,n\ ),$$

$$[u]_t^k = u_t^{k\,c} - u_t^{k\,a}.$$

where «* " is the tangential displacement on the side k, $(p_n^+)^k$ denotes the tensile strength, c^k is the shear strength, V is the set of displacements that fulfill the kinematical boundary conditions and condition (8). If p* = 0 then set K is a cone of admissible displacements satisfying the essential boundary and contact conditions. This is valid for brittle or almost brittle material (coal seam, glass). If the material exhibits elastic-plastic behavior, then the cone K is changed as:

$$K = (u \in V, (p_n^+)^k \ge p_n^k = k_n^k[u]_n^k,$$

$$\text{if } (p_n^+)^k \le p_n^k \text{ then } p_n^k = 0$$

$$k_t^k |[u]_t^k| \le c^k \chi(p_n^k) - p_n^k \tan\phi \text{ on } \Gamma_C^k, \quad k = 1,\dots,n \ ),$$

$$[u]_t^k = u_t^{k,\alpha} - u_t^{k,\beta}.$$

where ϕ is the angle of internal friction, and $p^k{}_n$ is the normal traction on the side k, x 's me generalized Heaviside's function being equal to zero for a positive argument and equal to one otherwise. Here the sign convention is important: positive normal traction is tension.

From the above-defined spaces we can deduce that $p_n^k, [u]_n^k$, and $p_t^k, [u]_t^k$ behave linearly between certain limits, which are given by the material nature of the body.

The total energy J of the system reads:

$$J(u) = \frac{1}{2}\, a(u,u) - \sum_{k=1}^{n} \int_{\Gamma_C} (k_n^k ([u]_n^k)^2) d\Gamma - \int_{\Omega} b^T u d\Omega \quad (9)$$

$$a(u,u) =$$

$$= \int_{\Omega_\vartheta} \varepsilon^T C \varepsilon d\Omega_\vartheta, \varepsilon = (\frac{\partial u_n}{\partial x_n}, \frac{\partial u_t}{\partial x_t}, \frac{1}{2}(\frac{\partial u_t}{\partial x_n} + \frac{\partial u_n}{\partial x_t})).$$

where e is the strain tensor, C is the stiffness matrix of the particle, T denotes transposition, Ω_ϑ is the sum of subdomains Ω, i.e., of hexagonal elements, b is the volume weight vector.

Note that the spring stiffness $k[$ plays the role of a penalty. Recall that the problem can also be formulated in terms of Lagrangian multipliers, and then leads to mixed formulation. The latter case is more suitable for a small number of boundary variables; the problem discussed in this thesis decreases the number of unknowns introducing the penalty parameters.

FORMULATION OF TFA

In this section, our aim is to formulate the general procedure for the TFA. This may be done in terms of many modem numerical methods. It seems that the BEM is the most appropriate numerical method in this case, but the FEM is also admissible.

First, let us consider that the body (part of a structure, element, system of more elements, composite) behaves linearly; i.e. Hooke's linear law is valid in entire body (this assumption admits among others an application of the BEM). When the problem is correctly posed, the displacement vector, strain and stress tensors can be obtained from the Navier equations, kinematical equations, and the linear Hooke's law.

In the second step we select points, where the measured values are available, either from experiments in laboratory, or from "in situ" measurements. We also select points, or regions (subdomains) from the body under study, and apply there successively unit eigenparameter impulses (either eigenstresses or eigenstrains) to get an influence tensor (matrix). In order to precise this statement, denote A_i, i = l,...,n, either the points or regions where the eigenparameters will be applied. Let, moreover, the set of points where the measured values are known be S_j, j = l,...,m. Then the real stress at ß; is a linear hull of stress $a^{e\%\prime}$ at Bj due to external loading and eigenstrains n and e^{p_l}, or eigenstress X and relaxation stress 0^{rel} at A_t (similar relations are valid for overall strain field E):

$$\sigma = \sigma^{ext} + P^\sigma \mu + Q^\sigma \varepsilon^{pl}, \quad \text{or}$$

$$\sigma = \sigma^{ext} + R^\sigma \lambda + T^\sigma \sigma^{rel}, \quad (10)$$

$$\varepsilon = \varepsilon^{ext} + P^\varepsilon \mu + Q^\varepsilon \varepsilon^{pl}, \quad \text{or}$$

$$\varepsilon = \varepsilon^{ext} + R^\varepsilon \lambda + T^\varepsilon \sigma^{rel}, \quad (11)$$

or in differential (incremental) form:

$$d\sigma = d\sigma^{ext} + P^\sigma d\mu + Q^\sigma d\varepsilon^{pl}, \quad \text{or}$$

$$d\sigma = d\sigma^{ext} + R^\sigma d\lambda + T^\sigma d\sigma^{rel} \quad (12)$$

$$d\varepsilon = d\varepsilon^{ext} + P^\varepsilon d\mu + Q^\varepsilon d\varepsilon^{pl}, \quad \text{or}$$

$$d\varepsilon = d\varepsilon^{ext} + R^\varepsilon d\lambda + T^\varepsilon d\sigma^{rel}, \quad \textbf{(13)}$$

where the influence tensors P, Q, and R and T may be identical (in the case of the TFA they must be identical, as they describe generalized linear Hooke's law, and $\mu = \varepsilon^{pl}$, $\lambda = \sigma^{rel}$), as any eigenparameter may stand for the plastic or relaxation parameter (say, eigenstrain may stand for plastic strain, which is obvious from (1)). The dimensions of σ, σ^{ext}, μ, ε^{pl} λ, and σ^{rel} are m x 6 (because of symmetric stress and strain tensors) and the dimensions of P and Q are m x 6 x n. In the classical TFA the values of |x, or ε^{pl} are calculated from minimization of variance of computed and measured stresses. It holds: $\lambda = -C\mu$

The first relations in (10) and (12) describe the initial strain method while the second relations in

those equations formulate the initial stress method The eigenparameters may generally stand for plenty of phenomena like change of temperature, swelling, watering, etc. This is why we could split the eigenparameters in (10) into two parts: eigenparameters themselves and the quantities connected with physically nonlinear behavior of the material.

DISTURBED STATE CONCEPT (DSC)

The idea of this theory was originally proposed by Desai, and the theory characterized behavior of overconsolidated clays. Since then, Desai and coworkers have developed and successfully applied this concept to other materials (Desai 1994).

The DSC is a unified modeling theory for mechanical behavior of material and interfaces. It allows incorporation of the internal changes on interfacial boundaries of phases (both micro- and macrolevel) and the resulting mechanism in a deforming material into the constitutive description. Initially, the material under external loading is in relative intact state (IS). Using such theories as elasticity, plasticity and viscoplasticity may theoretically treat the intact state, i.e. no cracking is considered in this state. After increasing the external loading, the material transforms from the IS state to the fully adjusted state (FA) or critical state, which is an asymptotic state, the material at that may no longer carry certain or all stresses. For example, microcracking and subsequent softening are such disturbances.

Desai uses a scalar disturbance function *D,* having different expressions depending of mechanical properties in the model under consideration. The equilibrium equation for a material element in terms of stresses is derived as:

$$D_u S_{ij} = (D_u - D)\,\sigma^{IS}_{ij} + D\,\sigma^{FA}_{ij}\,, \qquad (14)$$

where S_{ij} stands for average (observed) response, D_u is max D and is in most cases equal to one. Using the incremental method, the differentiation of the last relation yields:

$$D_u\, dS_{ij} = (D_u - D)\, d\sigma^{IS}_{ij} + D\, d\sigma^{FA}_{ij} + dD\,(\sigma^{FA}_{ij} - \sigma^{IS}_{ij}) \qquad (15)$$

The first term of the right hand side of the last equation expresses continuum constitutive law for elasto-plastic (visco-plastic) behavior, the second term obeys the classical Kachanov damage formulation (Kachanov 1992), and the third term in (15) indicates different stresses in the two parts.

The incremental constitutive equations for the IS part and the FA part are expressed as:

$$d\sigma^{IS}_{ij} = C^{IS}_{ijkl}\,\varepsilon^{IS}_{kl}\,,\quad d\sigma^{FA}_{ij} = C^{FA}_{ijkl}\,\varepsilon^{FA}_{kl} \qquad (16)$$

where C^{IS}_{ijkl} are in our case the components of von Mises-Huber-Hencky constitutive tensor IS part, furthermore C^{FA}_{ijkl} are the components of damage constitutive tensor for FA part, superscripts IS and FA indicate the phases. For more details concerning the DSC see Desai's publications cited in References.

For Hooke's law with Mises condition involving eigenstrain it holds in incremental form:

$$\varepsilon_{ij}(du) = A_{ijkl}\, d\sigma_{kl} + d\,(\varepsilon_{ij})^{pl} + \mu_{ij}\,, \qquad (17)$$

where (Duvant and Lions 1972):

$(\varepsilon_{kl})^{pl} = 0$ for $F(\sigma) < 0$ and

$(\varepsilon_{kl})^{pl} = 1/(2Gs)/(s - k)(\sigma_{ij})^{D}$ for $F(\sigma) > 0$,

$2s^2 = (\sigma_{ij})^{D}(\sigma_{ij})^{D}$

and $(\sigma_{ij})^{D}$ are components of deviatoric part of the stress tensor, $F(\sigma)$ is the function of plasticity, which is defined for Mises model as:

$$F(\sigma_{ij}) = \tfrac{1}{2}(\sigma_{ij})^{D}\,(\sigma_{ij})^{D} - k^2$$

In the last formulas G is the shear modulus, k is a material positive constant.

Using the dual transformation formulated by Duvant and Lions, we arrive at the following variational principle:

$$\int_{\Omega} [\frac{1}{2}\kappa(divu)^2 + \Phi(\varepsilon^{D})u)]dx - \int_{\Omega} f_i u_i dx - \int_{\Gamma_\sigma} p_i u_i dx$$

$$\Rightarrow \min, \qquad (18)$$

where

$\Phi(\varepsilon^{D}) = G(\varepsilon_{ij})^{D}(\varepsilon_{ij})^{D}$ for $2G^2(\varepsilon_{ij})^{D}(\varepsilon_{ij})^{D} < k^2$,

$\Phi(\varepsilon^{D}) = k\,((2(\varepsilon_{ij})^{D}(\varepsilon_{ij})^{D})^{1/2} - k/2G)$

for $2G^2(\varepsilon_{ij})^{D}(\varepsilon_{ij})^{D} > k^2$,

Ω is the domain with a boundary r, r_p is the part of /"where the tractions are prescribed, f is the function of volume weight, p are tractions, $(\varepsilon_{ij})^D = (\sigma_{ij})^D / 2G$ are components of the strain deviatoric tensor and K is the bulk modulus. The minimum of the functional is sought for such displacements u, which fulfil! the geometric boundary conditions.

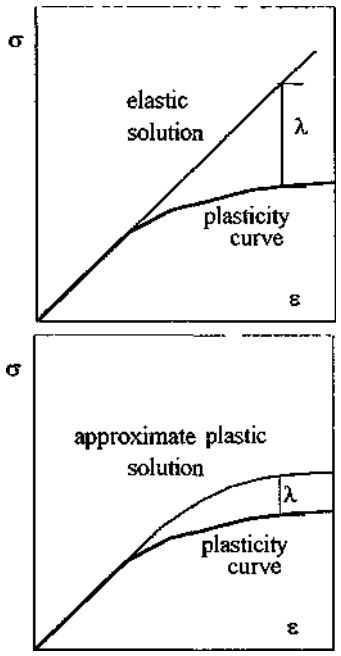

Figure 2. TFA model and unified DSC & TFA model

In order to make more transferable the TFA and the improved concept using Desai idea, a uniaxial stress-strain distribution is depicted in Figure 2. One can observe that first the elastic problem is solved, where even not too precise values of material properties are required. From the second picture in Figure 2 it is seen that nonlinear material behavior is estimated and the relaxation stresses improve the constitutive law in accordance with measurement.

TFA & DSC CONCEPT

Recall first the TFA involving the DSC. The transformation field analysis consists of expressing the stress σ at an arbitrary point ξ of the domain by virtue of superposition of stress $\sigma^{ext}(\xi)$ at ξ due to external loading which is applied to a plastic, viscoplastic, or others matrerials, and a linear hull of, say, the eigenstresses λ_1 and plastic strains ε^{pl} at other points x. Since we assume that at each point six values of stress, plastic stress, and eigenstress tensors are prescribed, the relation stresses σ^k at the points S^*, k = 1,...,m, and the eigenstresses and plastic stresses λ_1^l, l = 1,...,n and $(\sigma^{pl})^l$, l = 1,..., m at *Ai* becomes (to simplify the expressions the vector notation for stress and strain tensors is used), cf. (1):

$$(\sigma_i)^k = (\sigma^{ext}{}_i)^k + \sum_{j=1}^{6} \sum_{l=1}^{m} (R^{\sigma}{}_{ij})^{kl} (\lambda_j)^l + \sum_{j=1}^{6} \sum_{l=1}^{m} (T^{\sigma}{}_{ij})^{kl} (\sigma^{rel}{}_j)^l, \quad i = 1,...,6, \; k = 1,...,m, \quad (19)$$

or

$$(\sigma_i)^k = (S^{\sigma}{}_i)^k + \sum_{j=1}^{6} \sum_{l=1}^{n} (R^{\sigma}{}_{ij})^{kl} (\lambda_j)^l, \quad i = 1,...,6, \; k = 1,...,m, \quad (20)$$

where $(S^{\sigma}{}_i)^k$ express the current state of the overall stresses involving nonlinear changes in the material.

Note that similar relations can be written for displacements:

$$(u_i)^k = (u^{ext}{}_i)^k + \sum_{j=1}^{6} \sum_{l=1}^{m} (R^{u}{}_{ij})^{kl} (\lambda_j)^l + + \sum_{i=1}^{6} \sum_{l=1}^{m} (T^{u}{}_{ij})^{kl} (\sigma^{rel}{}_j)^l, \quad i = 1,...,6, \; k = 1,...,m, \quad (21)$$

or

$$(u_i)^k = (S^{u}{}_i)^k + \sum_{j=1}^{6} \sum_{l=1}^{n} (R^{u}{}_{ij})^{kl} (\lambda_j)^l, \quad i = 1,...,6, \; k = 1,...,m. \quad (22)$$

On the other hand measured stresses $(\sigma_i^{meas})^k$, or measured displacements $(u^{meas}{}_i)^k$ are available in a discrete set of points. A natural requirement is that the values of measured and computed values be as close as possible. This leads us to the optimization of an "error functional"

$$I[(\lambda_j)^l] = \sum_{i=1}^{6} \sum_{k=1}^{m} [(\sigma_i)^k - (\sigma_i^{meas})^k]^2 \rightarrow \text{minimum}, \quad (23)$$

or

$$I[(\lambda_j)^l] = \sum_{i=1}^{6} \sum_{k=1}^{m} [(u_i)^k - (u_i^{meas})^k]^2 \rightarrow \text{minimum} \quad (24)$$

Differentiating / by $(\lambda_\alpha)^\beta$ yields a linear system of equations for $(\lambda_j)^l$:

$$\sum_{j=1}^{6}\sum_{l=1}^{n}(A_{\alpha\beta})^{\beta}(\lambda_j)^l = Y_{\alpha}^{\beta},\quad \alpha=1,\ldots,6,\ \beta=1,\ldots,m, \tag{25}$$

where

$$(A_{\alpha\beta})^{\beta} = \sum_{i=1}^{6}\sum_{k=1}^{m}(R_{ij})^{kl}(R_{i\alpha})^{k\beta},$$

$$Y_{\alpha}^{\beta} = -\sum_{i=1}^{6}\sum_{k=1}^{m}(S_i)^k\cdot(u^{meas}{}_i)^k +$$

$$+\sum_{j=1}^{6}\sum_{l=1}^{m}(R_{ij})^{kl}(\lambda_j)^l(R_{i\alpha})^{k\beta}$$

In order to get d(o;/ in (8), one needs to calculate $d(\lambda_j)^l$. This is the difference between $(\lambda_j)^l$ from (11) and the same quantities from the previous step of incremental method.

The procedure deserves a closer attention. In the first step the influence matrices are created, as described in the above explanation (Sect, on formulation of the TFA). The distribution of the disturb function D is determined mostly from laboratory tests. The incremental method is recommended when applying the DSC & TFA.

Let us start with some load of the trial body.

At the beginning the FA state will be most probably not reached. The Intact State follows the von Mises-Huber-Hencky law. When increasing the load, the DSC has to involve both IS and FA states into the computation. Then, the stresses are split into IS and FA parts. Increments of both these parts can be done from the DSC and the total stress for both parts is given by adding the increments to the previous steps. The same is valid for the total current stress; see (7).

Since the relations (20) and (22) are linear, substitutions of $(S_i f$ and $(\lambda_i)^k$ there do not change the linearity. Then applying the minimum condition for the additional eigenstresses, the improvement of current stresses or error for the DSC is obtained.

The above-described procedure can be created for measured displacements in a similar way. The displacements have to substitute overall stresses and the "error functional" has to be employed. This is not in the full compliance with classical Transformation field analysis, but it follows from mechanical point of view.

CLASSICAL CONTINUUM DAMAGE MODEL

In the previous section, λ_1 was used to express "error function", improving the choice of plasticity model. The function λ_2 will express the influence of the damage.

In the continuum damage model it is assumed that the damaged parts can carry no stress at all, and they act as voids. In other words, the observed response derives essentially from the undamaged parts; their stress-strain-strength behavior is degraded because of the existence of the damaged parts. For example, the damage parameter, ω, is defined as

$$\omega = 1 - \frac{V^V}{V}$$

where V is the volume of the damaged parts and V is the total volume of the material element. Then, $\omega = D$ represents the special case and appears in X_2 as an argument.

In the sense of the Unified TFA & DSC Concept the equilibrium for d a can be written as

$$\sigma = \sigma^{IS} - \lambda_2(\omega),$$

The representation of the function of $\lambda_2(\omega)$ can be found in (Kachanov 1992), for example.

In comparison to simple TFA & DSC, the involvement of free hexagons leads to nonlinear equations because of impossibility defining an appropriate cone. On the other hand, this approach seems to be very promising, as it offers one of the most efficient procedure leading the minimum variance of measured and computed results. The expressions (19) and (21) together with variational principle (23) enable us to connect both types of measurement.

DISCUSSION OF THE RESULTS

The material values has been selected as

Fibers: $E_r = 414$ GPa, $v_f = 0.19$, $c_f = 0.25$

Matrix: $E_n = 99.5$ GPa, $v_{ra} = 0.3$

$F^{TM}{}_{mres}{}^{*} = 48.7$ GPa, $v_{mres} = 0.42$

$k^2 = 510$Mpa

where c_f is the fiber volume fraction. Two-dimensional case is solved. Because of symmetry, overall strain has been applied in two directions: $E_n md\ E_{l2}$- The responses in damage (debonding of matrix from fibers) and plastic zones are calculated and depicted in Figs. 4b and 4c. The debonding corresponds a typical "75° zones along the interfacial boundary while plastic zones creating tongues between fibers. They are relatively long, as the plastic zone is limited by relatively low value of k.

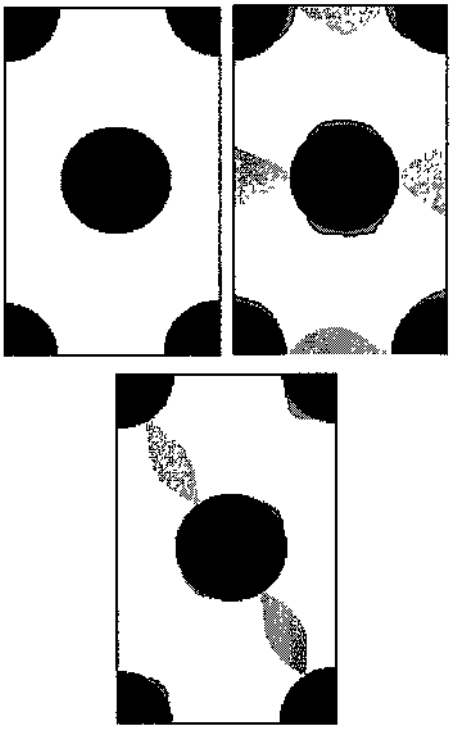

Figure 4. Damage and plastic behavior of rectangular RVE in periodic fibers: a) Geometry of the RVE, responses of b) E_n and c) E_n •

CONCLUSION

Generalized transformation field analysis is improved by Desai's DSC. In the model, damage is involved in a natural way using eigenparameters, which are known from classical TFA. They represent either plastic strains in Desai's model and play role of "error function", showing how exact the model and material parameters are selected; also describe the damage properties involved in Unified model. The results correspond the classical damage (debonding) behavior. The plastic behavior follows a concentration of stresses in the zones describing the plasticity.

4 CONCLUSIONS AND REFERENCES

Acknowledgment: This paper has been prepared under financial support of GACR, project No. 103/03/0483 with the title 'Tunnel face stability by Transformation Field Analysis and Distinct State Concept".

REFERENCES

Bittnar, Z & Sejnoha, J. 1996. *Numerical methods in structural mechanics.* ASCE Press, New York

Cundall, P.A. 1971. A computer model for simulation progressive large-scale movements of blocky rock systems. *Symposium of the international society of rock mechanics:* 132-150

Desai, CS. (ed. H. Mulhaus) 1994, Constitutive Modeling Using the Disturbed State Concept, Chapter 8, *Continuum Models for Materials with Microstructure.* John Wiley & Sons, London, UK

Dvorak, G.J. 1992. Transformation Field Analysis of inelastic composite materials. *Royal Society of London* A437: 311-327

Dvorak, G.J. & Prochâzka, P. 1996. Thick-walled Composite Cylinders with Optimal Fiber Prestress. *Composites, Part B,* 27B: 643-649

Dvorak, G.J., Prochâzka, P. & Srinivas, S. 1999. Design and Fabrication of Submerged Cylindrical Laminates, Part I and Part II. *Int. J. Solids & Structures:* 1248-1295

Duvant, J. & Lions, J.P. 1972. *Variational Inequalities in Mechanics.* DUNOD, Paris

Kachanov, L.M. 1992, *Introduction to Continuum Damage Mechanics.* Martinus Nijhoff Publishers, Dordrecht, Netherlands

Michel J.C. & Suquet, P. 2003. Nonuniform transformation field analysis. *Int. J. Solids & Structures* 40: 6937-6955

Moreau, J.J. 1994. Some numerical methods in multibody dynamics: Application to granular materials. *Eur. J. Mech.Sohds,* 13, (4): 93-114.

Onck, P. & van der Giessen, E. 1999. Growth of an initially sharp crack by grain boundary cavitation. *Jour. Mech. And Physics of Solids* 28: 328-352

Prochâzka, P. 2004. Application of Discrete Element Methods to Rock Bumps. *Engineering Fracture Mechanics,* 45: 254-267

Prochâzka, P. & Trckovâ, J. 2000. Coupled modeling of Concrete Tunnel Lining. *Our World m Concrete and Structures,* Singapore: 125-132

Prochâzka, P. & Trckovâ, J. 2001. Coupled modelling using DSC&TFA theoretical process. Proc. *Computer methods and advances m geomechanics.* Virginia, USA, A. A. Balkema: 389-394

Trckovâ, J. & Prochâzka, P. 2001. Coupled modeling of tunnel face stability. Proc. *ISRM 2001 - 2nd ARMS,* A.A.Balkema Publishers: 283-286

Evaluation of the Relationships Between P-Wave Velocity *(Vp)* and Joint Density (J„)

R Altındağ
S D U Engineering and Architecture Fac, Department of Mining Engineering, 32260 İsparta, Türkiye

A Guney
Muğla University, Faculty of Engineering, Department of Mining Engineerings 48000 Muğla, Türkiye

ABSTRACT: Certain parameters such as rock type, density of joints, unit volume weight, porosity, amsotropy, weathering, temperature, water content, gram size and shape etc have direct effect on the values of seismic velocities

In this research, the trend of quantitative effect of joints on *P* waves *(Vp)* was investigated m laboratory since rock properties are greatly affected by the presence of discontinuities in the medium Therefore, prismatic rock samples of different thicknesses were prepared from a total of four different rock types, three of sedimentary and one of metamorphic origins For each rock type, set of samples with artificial joints were formed by adjoining several pre-sawn samples of different thicknesses, 1 to 6, and *Vp* values were measured The relationships between the number of joints and *P wave* velocities were statistically investigated and the results were assessed together with the results found in literature

1 INTRODUCTION

Seismic techniques are widely used in laboratory and as well as m the field in order to determine the dynamic properties of rocks In underground mining, seismic methods are often employed to predict stress re-distnbutions which induce break zones around underground openings This technique is also widely used to establish the blast-hole pattern m open pit mining and to determine fracture patterns in marble quarries to enhance block productivity

Various researchers have produced meaningful results by investigating the relationships between rock properties and seismic velocities Kahraman (2001) has carried out seismic velocity measurements on six different rock types (2 of granites, 3 of travertines, 1 of marble) containing three artificial joints and reported that *Vp* values decreased as the number of artificial joints increased, suggesting an inverse relationship between the *Vp* and the number of joints (J_N) Muftuoğlu (1990) has conducted a research to determine whether seismic velocities can be correlated with the spacing between the discontinuities in rock mass and has concluded that although the solution to this problem is difficult and complicated there is a limited solution

The evaluation of joints (frequency, trace length and orientation of joint sets) bears great importance in rock mechanics since shape of the block, their volume in the rock masses and their mechanical strength (compression and shear strength, deformation modulus, etc) are all affected by joint density in rock masses The degree of jointing is directly affected at the outcrops using scanhnes or on drill cores by means of Rock Quality Designation (RQD) (Deere, 1963), providing a direct block size measure Sjugren et al (1979) and Palmstram (1995) proposed two hyperbolic correlations linking respectively the unıdımensıonal joint frequency and the RQD to in situ longitudinal wave velocity (Vp)

2. LABORATORY STUDY

In the scope of this study, four different rock types were investigated (Table 1) Some of the physical properties of the rocks were determined m compliance with the ISRM (1981) and displayed in Table 2 A number of block samples in size of 10x10x35 cm were prepared and *P wave* velocities

were measured on each block prior to sawing. Later, the samples were sawn off the blocks in thicknesses of 1,2,3,4,5,6 and 7 cm in order to form sets of test samples with consecutive artificial joints varying in number between 0 to 6 as shown in Figure 1. Contact surfaces of the sawn-off samples were polished sufficiently for smooth planes. A good coupling along the contact surfaces of joints was satisfactorily maintained even in the absence of vertical load by carefully clamping sample sets at the ends. Then, *P-wave* velocity measurements were conducted on the sample sets by Ultrasonic Testing Equipment with 54 kHz frequency. The results of the measurements depending on the number of joints were illustrated in Table 3.

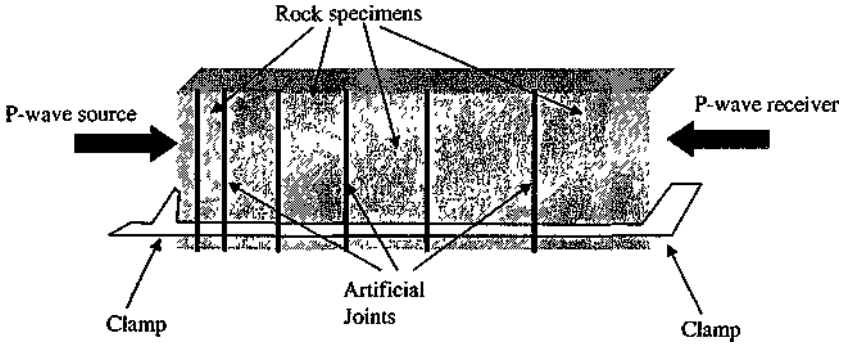

Figure 1. Schematic view of a sample set with six artificial joints

Table 1. Some characteristics of the rocks tested

Code Number	Rock Type	Rock Class	Bedding
1	Limestone	Sedimentary	Present
2	Limestone	Sedimentary	Present
3	Limestone	Sedimentary	Present
4	Marble	Metamorphic	Absent

Table 2. Physical properties of rocks

Code Number	Density (g/cm^3)	Effective Porosity (%)	Shore Hardness (SH)	Pre-sawn *VpO* (km/s)
1	2.72	9.06	41.9	5.752
2	2.69	7.37	52.8	5.334
3	2.85	0.84	46.5	5.040
4	2.66	11.74	29.1	4.963

3. STATISTICAL ANALYSIS

The sound velocity test results were analysed using the least squares technique. The equation of the best-fit line, the 95% confidence limits, and the correlation coefficient (r) were determined for each regression.

For each rock type, P-wave velocities and the number of artificial joints were correlated. The plots of the number of joints as a function of the *P*-wave velocities and the reduction rates in *Vp* with increasing number of joints (JN) are shown in Figures 2-5. It can be noted that there are inverse linear relations between the number of joints and

the P-wave velocities for each rock type. The P-wave velocity decreases as the number of joints increases. The regression equations and the correlation coefficients are given in Table 4.

Table 3. The results of P-wave velocity measurements

Code Number	Number of Joints *(JN)*	P-wave velocity (km/s)	Rate of Reduction in Vp with an increase in *JN* **(%)**
1	0	5.752 (Vpo)	100
	1	4.803	84
	2	4.436	77
	3	3.731	65
	4	2.168	38
	5	1.514	27
	6	0.701	12
2	0	5.334 (*Vpo)*	100
	1	3.400	64
	2	2.777	52
	3	1.872	35
	4	1.661	31
	5	1.289	24
	6	1.238	23
	7	0.685	13
3	0	5.040(*Vpo)*	100
	1	3.984	79
	2	2.767	55
	3	2.666	53
	4	2.241	44
	5	1.578	31
	6	1.176	23
4	0	4.963(*Vpo)*	100
	1	4.118	83
	2	4.014	80
	3	3.932	79
	4	3.131	63
	5	1.196	24
	6	0.941	19

Table 4. Regression equation for each rock type*

Code Number	Equation	Correlation coefficient
1	/AT=-1.1441 *Vp* + 6.7763	*r*= -0.990
2	J_N= -1.5019 *Vp* + 6.9271	r=-0.927
3	J_N =-1.5563 *Vp* + 7.3248	r=-0.970
4	J_N= -1.3168 *Vp* + 7.1942	r=-0.940

* J_N = Number of joints, *Vp* = P-wave velocity (km/s).

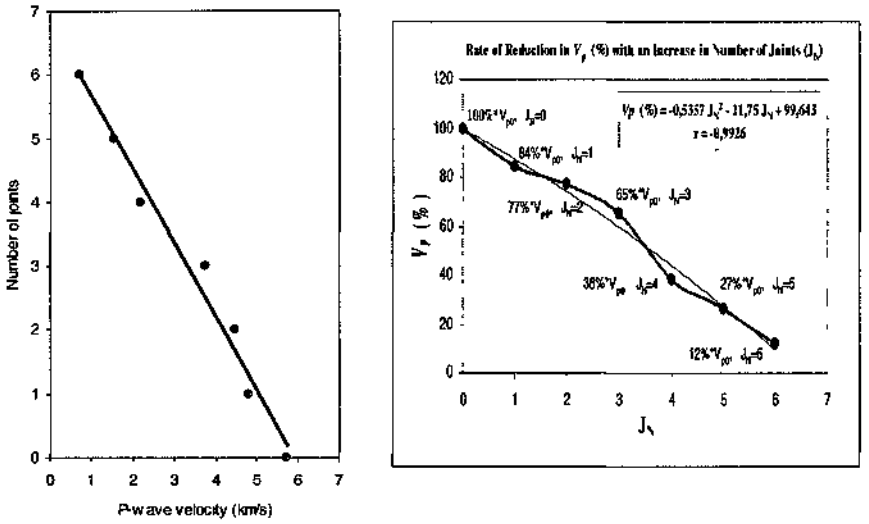

Figure 2. (a) J_N vs. *Vp* (b) *Vp* reduction rate (%) as J_N increases for rock code 1.

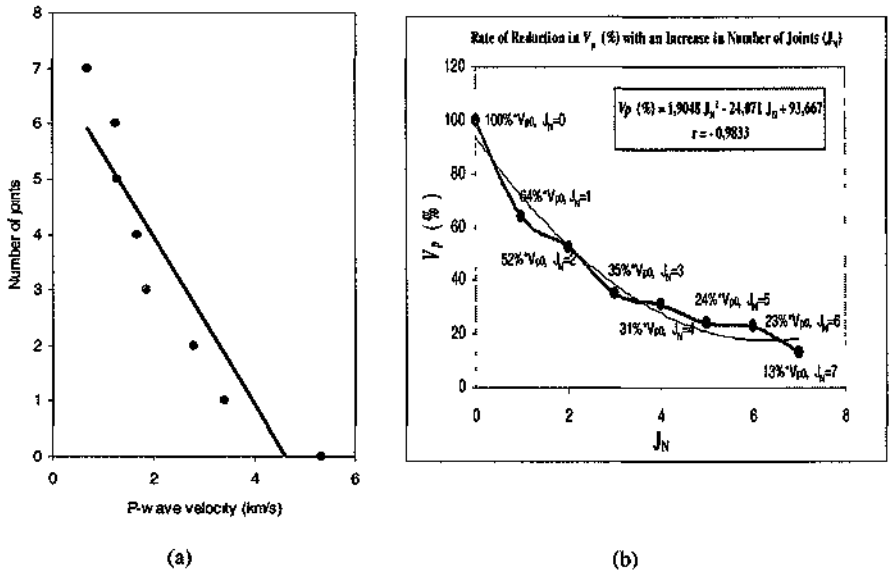

Figure 3. (a) J_N vs. Vp (b) *Vp* reduction rate (%) as J_N increases for rock code 2

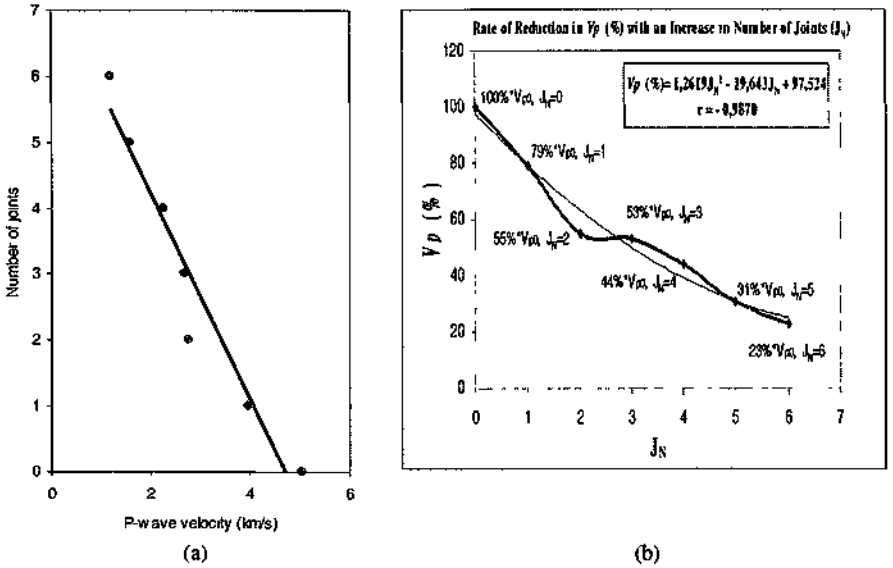

Figure 4. (a) JN VS. *Vp* (b) *Vp* reduction rate (%) as JN increases for rock code 3

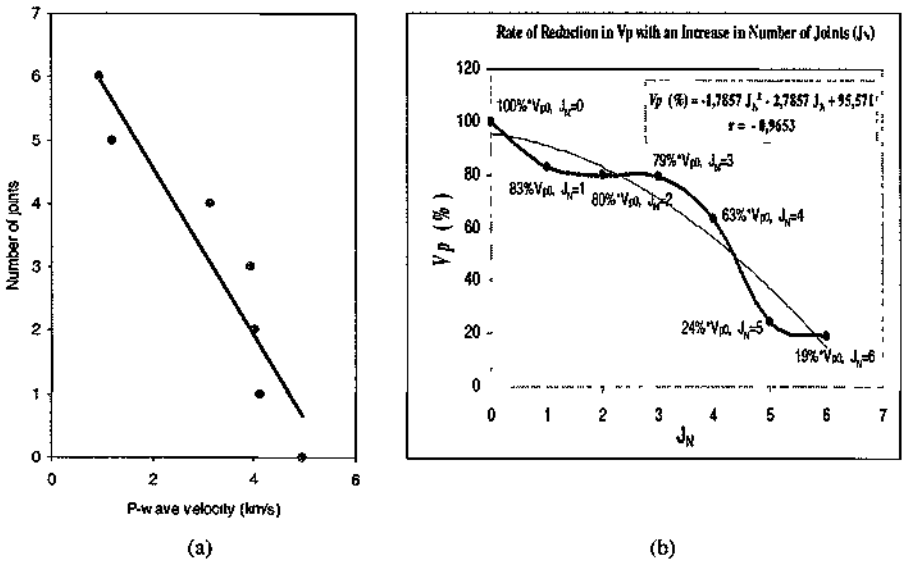

Figure 5. (a) J_N vs. *Vp* (b) *Vp* reduction rate (%) as JN increases for rock code 4

4. CONCLUSION

As well known, the degree of jointing, which is one of the most important parameters influencing seismic velocities in rock mass must be considered by researchers and engineers when designing structures m rock masses Therefore, the effect of joint density on seismic velocities were investigated on four different rock types associated with artificial joints as many as 6 The results of the experiments confirm that *P-wave* velocity decreases with an increase in the density of joints in rocks, agreeing with the results obtained by Kahraman (2001) Furthermore, there is a good polynomial correlation between the number of joints and the reduction rates in *Vp (%)* indicating that *P-* waves are attenuated rapidly as the number of joints increases

This study needs further laboratory investigation to clarify the effect of degree of jointing on seismic velocities by assessing the origins of the rocks and other significant rock physical properties

5. REFERENCES

Deere D U, 1963, Technical descnption of rock cores for engineering purposes *Felsmech Ingemurgeol,* 1, 16-22

ISRM, 1981, *ISRM Suggested Methods Rock Characterization Testing and Monitoring* Oxford Pergamon Press

Kahraman S, 2001, A correlation between P-wave velocity, number of joints and schmidt hammer rebound number, *bit J Rock Mech & Min Sei*, 38, 729-733

Muftuoğlu V M, 1990, Sismik hız ile eklem tıpı süreksizliklerin saptanabilirliği Kaya Mekaniği Bülteni 4, 19-36, 1990

Sjögren B, 0usthus A, Sandberg, I, 1979, Seismic classification of rock mass qualities *Geophys Prospect,* 27 (2), 409-442

Palmstr0m, A , 1996, Characterizing rock masses by the RMi for use in practical rock engineering, Part I The development of rock mass index (RMi) *Tunnelling Underground Spac e Technology,* 11, 17

3R - Rock Related Risk Management System for Mines

K S Koldaş
Omya Mining, Istanbul - Turkey

ABSTRACT Increasingly, raining regulatory bodies are requiring mine operators to base their health and safety assurance on the issue of risk assessment This is because it is now well recognised that risk assessment is an ideal process on which to build a pro active safety management system that can lead to dramatic improvement m safety and health performance A high incidence of rock related 'falls of ground' accidents prevail in many mines Although it is known but not yet applied in many mining industry in Turkey the risk assessment issue has been legalised and an inevitable part of mine management in many countries In this study, the author firstly described the concept of nsk management system and adopted into rock engineering principles in order to improve productivity and safety in mines

1. INTRODUCTION

It is true that mining is a risky business both in terms safety and economic point of views In order to mitigate the consequences and frequency of the risks in mining industry one should definitely consider in on risk assessment process On the other hand mining regulatory bodies in many developed countries are requiring mine operators to base their health and safety assurance on the use of risk assessment This is because it is now well recognised that risk assessment is an ideal process on which to build a pro active safety management system that can lead to dramatic improvements in safety and health performance

2. RISK ASSESSMENT CONCEPT

Risk assessment is a systematic examination of any activity, location or work process to identify risks to system success, understand the likelihood and potential and potential consequences the threat to success or hazards and review the current or planned approach to controlling the risk, adding new potential controls where required System success is defined by safety, health, production, environmental protection, community acceptance, security, or, m quality terms, optimal output with minimal waste

There are two distinct approaches to the assessment of risk quantitative and subjective Quantitative risk assessment has its origins in the high technology process industries, where it is used principally to assess risks associated with major accident hazards In quantitative risk assessment, numerical probabilities of risk are calculated using various sources of engineering data, and compared against a pre-set value of acceptance Rigorous and relatively complex formal hazard identification techniques, such as fault trees and event trees are used In subjective risk assessment, which is more commonly used within lower technology industries estimates of risk are based on subjective judgements of likelihood and severity The judgements of likelihood and severity are based on some form of subjective scales and often, less formal hazard identification techniques are employed

Whichever risk assessment technique is used, it is important to remember that the true purpose of introducing such a process is to improve health and safety In most cases, times consuming quantitative techniques are neither practical nor necessary to achieve this end result

3-ROCK RELATED RISK MANAGEMENT-3RM

One stated that *'the first principal duty of business is to survive and the guiding principles of*

business economic? is not the maximize of profit - it is the avoidance of loss'

During the last few decades a great deal of effort has been Jevoted to the development of rock mechan ;> as applied to engineering The basic principles of the subject have been established and a variety o methods and tools specifically relevant to this fled of application have been developed

When we start to examine the safety statistics of many mines we obviously reckon that most of the accidents occur as a result *of falls of ground, lack of or inappropriate support units, lack of excavation & blasting design* as well as rock engineering knowledge etc The source mechanism of all these types of accidents are of course *rock related* Because we all mining engineers deal with rock and have moral obligations to safety of workforce we must adopt and develop some sort of rock engineering risk assessment techniques in order to combat rock-related hazards in mines

In mining, rock mechanics has become an important tool in planning the layout of open pit and underground mines, in the evaluation of support requirements, in the alleviation of mining hazards and in making various technical decisions Therefore rock-engineering professionals can make a major contribution to both safety and profitability of mines

The rock-related nsk management provides the basis for decision -making and enables management to create a safer environment The principal purpose of rock-related risk management system is as follows (DME, 1996)

» Identify and describe rock related hazards, which are likely to arise from the mining of each geotechmcal area identified
- Assess and prioritise the health and safety risks to which workers will be exposed and record findings
- Develop and implement reasonably practicable strategies to reduce and manage these risks, based on above risk assessment and accident analysis
- Record the significant hazards to cerate safer and long term establishment

We can develop three types of rock-related risk assessment techniques in mines, which are namely (SIMRAC, 1997)

/ *Base line Risk Assessment*

This will be done to identify major risk for future risk control such as analysis of historical data, accident reports, internet, information, sharing info between mines etc These studies need to be comprehensive, and may well lead to further, separate, more m-depth risk assessment studies

2 Issue Based Ri sk A sse ssment

As circumstances and needs arise, separate risk assessment studies will be conducted when, for example a new support is introduced into the mine, after an accident or near miss incident, new knowledge comes into to light and information is received which may influence the level of risk to employees at the mine etc The suppliers m mines must ensure, as far as reasonably practicable, that the article is safe and without risk to health ad safety when used properly

3 Continues Risk Assessment

This is the most important for all of risk assessment, which will take place continuously, as an integral part of day-to-day management of the mine This will mainly be used by the front line supervisors in the mine, for example checklists, audits, planned task observations, daily workplace inspection etc

The baseline risk profile for rock engineering is presented in Table 1, followed by the risk-ranking scheme used for this overview This profile will help define the objectives of the mine's rock-engmeennng department, against which achievement targets will be set and reviewed It also highlights the rock related safety issues that need to be addressed by other departments m the future

After a baseline risk profile has been established highest priority risk areas are addressed in more detailed risk assessment The method, which has been used widely in mines, is the *WRAC (Workplace Risk Assessment and Control)* technique, Table 2 Using this technique, assessment can be done by a group or vertical slice of people from the workplace ranging from the person undertaking a given task to a higher level supervisor and is facilitated by personnel from rock Engineering Department

Hazards are identified by considering each step m the completion of a task and ranking the risk according to the *probability* of an incident happening and the likely *consequence,* as indicated by the risk ranking matrix illustrated in Table 1

Table 1.Risk Matrix-f (CxP)

	PROBABILITY				
CONS.	A	B	C	D	E
Fatality-1					11
Serious Injury-2			8	12	16
Disabling Case-3		9	13	17	20
First Aid Case-4	10	14	18	21	23
No Injury-5	15		22	24	25

PROBABILITIES: This is normally a compound of two separate factors. Firstly, exposure, which is an analysis of how often and for how long the employees involved, is exposed to the hazard. Secondly, it includes an analysis of **probability,** that is the chance that a person or persons will be harmed during the exposure period. Common- (Daily)-A, Likely- (Weekly)-B, Happens- (Monthly)-C, Unlikely- (Yearly)-D, Rarely (1-3 years)-E

CONSEQUENCES: Here, the degree of harm from the identified hazard is assessed in terms of the potential severity of the injuries or ill health and/or the number of people potentially affected. (Fatality-1, Serious injury-2, First aid case-3, No injury-4)

A risk ranking of 1 is the most serious and 25 the least serious. Thus all rankings from 1 to7 are critical and require urgent consideration, rankings 8 and 15 are serious and 16 to 25 are of lesser severity and should be addressed only when the more serious risks have been eliminated or controlled.

3.1 Risk **Control** Measures

The risk assessment team should consider the following strategies and make recommendations to the manager:

Elimination
This can be done by either removing the hazard from the working environment, or by working in a different area.
Control the Risk at Source
This strategy may involve limiting access to the hazardous area, or by guarding against the hazard, or by operating from a remote distance.
Minimise the Risk
This strategy involves aspects such as hazard awareness training programmes to ensure that workers keep away from the hazardous areas and the use of safety devices.

High frequency and high consequence hazards are the highest priority. Those with a low frequency and low consequence are low priority and those with both high frequenc; and low consequence, or high consequence aid low frequency are considered as medium priority.

Personal Protective Equipment and Monitoring of the Risks
This approach should be the last resort to risk control.

Table 2. Example of risk assessment using the WRAC techniques in mines

Step	Hazard	P	C	R	System	RP
Application of support standards	Unsafe working areas	-	-	-	Codes of Practice	ME

When the current system fails or is insufficient then *recommended action* needs to be developed in order to eliminate risk.

3.2 Reporting and Recording of significant risks

All risk assessment exercises should be recorded by the rock engineer professional and must be easily accessible to all concerned. However, the documentation system should not detract from the major purpose of risk assessment and that is to improve the management of risks, thereby ensuring the health and safety of employees. The following aspects should be reported on:

* The major hazards identified.
- A review of the existing safety measures and the extents to which they work in controlling risks.
- Those who may be affected by the major hazards.

3.3 Preventative and Protective Measures

If possible, risks should be eliminated. If this is not possible, and then they should either be mitigated/controlled or minimised or, if none of these is possible, then personal protection should be provided. In deciding upon the types of preventative and protective measures that need to be provided, the following principles should be considered by the manager

- It is always best, if possible, to avoid a risk altogether. This can be done by using a different approach, substance or method of

work.

- Combat risks at source rather than by adopting secondary measures.
- Where' -r possible, work should be adapted to the ' .dividual rather than the individual adapted to the work.
- Make use of technological and technical progress when treating risks.
- Collective protection measures should be given priority.
- Protection provided should be backed up with adequate training and supervision.
- Measures to avoid, prevent and reduce risks need to be an accepted part of the approach and attitudes at all levels of the organisation.

3.4 **Other methods of hazard identification**

A number of hazard identification methods exist, most of which are implicit in the methods in section 3.

A number of methods are based on prior experience. These include (Koldaş, K.S, 1998): -

1. Accident analysis, major incident reviews and near miss analysis from which commonalties can be identified.
2. Members of the team may have been involved with investigations or have read accounts of incidents and, from personal experience and memory, are able to list factors.
3. Codes of practice, standards and working procedures are generally designed to prevent losses and their analysis can uncover expected hazards and incidents.
4. Safety and loss control audits may explicitly identify hazards ad incidents arising therefrom.
5. From imagination techniques such as brainstorming, scenarios are developed in which previously un-encountered incidents are created within a specific hazardous environment.
6. *'Cause-consequences'* methods rely on a systematic analysis of a given scenario such as a *'fault tree', 'event tree',* 'failure mode-effect and critically analysis (FMECA), the hazard and operability study (HAZOP).

3.5 Rock **engineering, hazard identification in strategic planning**

The objectives of any strategic planing process are twofold; the first is to identify a suitable strategy to meet the requirements of the particular problem. The second is to provide broad guidelines for detailed design work based on the chosen strategy.

Rock engineering input to strategic planing occurs in four main phases: -

1. Assisting in defining the requirements of the particular project.
2. Gathering relevant geotechnical information on conditions that will prevail
3. Assisting in generating alternative scenarios to meet the requirements defined in section 3.2
4. Assisting in selection of suitable scenario

An example of rock engineering input and hazard identification applied to strategic planning is such as shaft pillar, support design or remnant extraction.

3.6 Rock engineering and hazard identification process in operational planning and design

There are three main objectives of operational planning and design. Based on the information generated when defining the preferred strategy, the first objectives are to identify, in detail, hazards present and the incidents that could arise from them. The second objective is to identify methods of preventing or ameliorating the effects of those hazards and to incorporate those methods into the detailed design. The third objective is to provide guidelines for practice, procedures and specifications to control work during the operational phase.

The duties of the rock engineering service are to:

- review design and planning of new areas;
- review abnormal ground conditions and make proactive recommendations;
- review designated special areas and advice on requirements;
- participate in regular interdisciplinary mine planning and design meetings;
- initiate and implement monitoring, recording and reporting procedure;
- assist management with training in rock engineering aspects;
- assist management with investigation of serious rock related incidents;
- assist management with risk assessment of rock related issues;
- assist management with compiling and updating of the Code of Practice and

- assist management with the compiling and updating of Mine Standards.

3.7 Review **and** Revision

Risk assessment is a continuous process and as work changes, the hazards and risks may change and therefore the risk assessment process must also change. Risk assessments should be reviewed or modified when an accident occurs, or if more is learnt about certain hazards in the workplace. Thus, after an accident, the safety officer should select a risk assessment team and revisit the previous risk assessment to see:

- whether the accident which has occurred was predicted;
- « whether it was decided to prevent that accident;
- if so, why the preventative measures did not work;
- if the accident was not predicted, whether it is necessary to revise the risk assessment process or not;
- if the accident was predicted but it was decided to tolerate the risk, whether the decision was valid;
- why the accident occurred, and what should be done to prevent similar accidents occurring, as far as is reasonably practicable.

It is appreciated that the service provides maximum benefit if it is proactive and identifies potential hazardous conditions before they occur and create dangerous situations.

Rock engineering input to operational planing and design occurs in four main areas: -

1. Gathering detailed relevant geotechnical information relating to conditions that are likely to prevail; Table 3.

The geotechnical data, which should be collected, and recommended methods of collecting the data. Site investigations, geotechnical logging of borehole core, mapping of joints, rock mass classification mapping including recording of joint properties, and requirements for laboratory testing of rock samples are dealt with (SIMRAC, 1999).

- study of available geological plans and similar material;
- " remote sensing (satellite imagery);
- aerial photograph interpretation;
- specific field mapping;
- targeted exploration drilling, including specific geotechnical drilling, all based on the information obtained from the above investigations;
- evaluation and prediction of geological influences:
- structural;
- in situ and induced stresses;
- groundwater;
- quality and durability of the rock and rock mass;
- *m* control investigations during production, to identify conditions different from those on which the design was based.

2. Assisting in preparation of detailed micro layouts;
3. Assisting in generating macro sequences ad schedules;
4. Assisting in preparing codes of practice, operating procedures and specifications.

3.S The rock engineering and hazard identification processes **during operations**

During this phase there will be three main objectives of the hazard identification exercise: -

1. To generate awareness of hazard and their associated incidents amongst the workforce;
2. To monitor the effects of hazards in working places in order to allow timely intervention;
3. To provide information that will facilitate review and revision of practices, procedures and specifications.

Rock engineering input during operations consists largely of monitoring and observing conditions. It occurs in three main areas: -

1. To ensure that designs and methods for strata control are implemented correctly and are working effectively;
2. To identify any short, medium or longer term changes in geotechnical conditions which may demand modifications to procedures, practices or specifications and recommend appropriate action to deal with those changes;
3. To ensure that micro layouts are maintained and, if not, that the potential effects of deviations therefrom are

identified and appropriate action is implemented

Table 3 Example- Rock-related hazards associated with development in different rock types, (Koldaş, KS GCMP,2001)

ROCK TYPE	STRATEGIES
Hematitle Quartz Breccia	Hazard levels are increased for all rock types where tunnels and decline are developed or mined through faults and dykes due to presence of ground disturbed by jointing or smaller scale fracturing on the margin of these discontinuities Increase support density in all areas
Hydrothermal Breccia composed predominantly of andésite in a siliceous to silica clay matrix	Hazard levels are increased for all rock types where RQD values between 25 50% Steelarch units m conjunction with 2,4m grouted swellex + 50mm fibrecrete with wire mesh to be applied where poor ground and self mining conditions are intersected

3.9 Numerical Modelling

Numerical modeling provides excellent useful tools for assessing rock-related risks m mines Numerical modeling m rock engineering, as with almost computational analyses m traditional engineering disciplines, is based upon the assumption that the problem is well defined In realty this means that numerical modeling must be used to test proposed design specifications against well-established predefined criteria

4. CONCLUSION

Rock related risk management technique plays an ever increasing role in ensuring the safety and heath standard of mining operations The introduction of rock related risk assessment in mining industry presents a real opportunity to change and improve safety and health performance To do this successfully, it is vital that there is real commitment to change, to ensure that the process does not turn into yet another 'back protecting' paper exercise Rock related risk assessment requires a well-planned management system and rock-engineering professionals to ensure that improvements are implemented and to encourage widespread stakeholder participation

The mining industry throughout the world particularly in Turkey needs to improve its safety and health performance and it is therefore risk management process is an ideal opportunity to change the old culture

REFERENCES

DME, 1996 *Guideline for Compilation of a mandatory Code of Practice to Combat rockfall and Rockburst Accidents in South Africa,* Publication Ref No GME 7/4/118-AB2

Koldaş, K S 1998 Proposed Risk management Regulations for MRAC, *Department of Minerals and Energy Affairs of South Afuca*

Koldaş, K S 2001 GCMP *Rock Related Risk Assesemnt Studies in Newmont Ovacık Gold Mine*

SIMRAC, 1997 Practical guide to the risk assessment process, *Tupartite Woiking Group on risk Assessment*

SIMRAC, 1999 A Handbook on Rock Engineering Practice for Tabular Hard Rock Mines, Vol 1, pp 12-8